

AD-A102 335

ROCHESTER UNIV N Y LAB FOR LASER ENERGETICS
DEVELOPMENT OF X-RAY LASER MEDIA: MEASUREMENT OF GAIN AND DEVEL--ETC(U)
JUL 81 J M FORSYTH

F/G 20/5

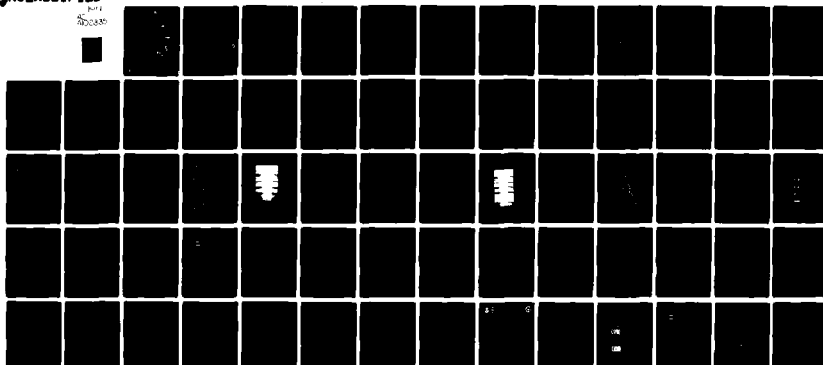
AFOSR-77-3189

AFOSR-TR-81-0613

NL

UNCLASSIFIED

500000



END
DATE
FILED
8-8-81
DTIC

AFOSR-TR-81-0613

LEVEL ✓

12
P.S.

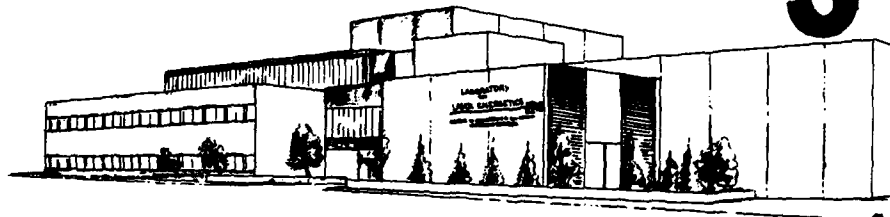
AD A102335

Final Technical Report

Air Force Office of Scientific Research

00077-3189

Development of X-Ray Laser Media:
Measurement of Gain and Development of
Cavity Resonators for Wavelengths ^{near}
130 Angstroms



DTIC
ELECTRONIC
AUG 3 1981
S C

DTIC FILE COPY

Laboratory for Laser Energetics
College of Engineering and Applied Sciences
University of Rochester
250 East River Road
Rochester, New York 14623

UR
LLE

Approved for public release;
distribution unlimited.

81 8 03 058

Unclassified

SECURITY CLASSIFICATION OF THIS PAGE (When Data Entered)

REPORT DOCUMENTATION PAGE		READ INSTRUCTIONS BEFORE COMPLETING FORM
1. REPORT NUMBER 18 AFOSR-TR-81-0613	2. GOVT ACCESSION NO. AD-A102335	3. RECIPIENT'S CATALOG NUMBER
4. TITLE (and Subtitle) DEVELOPMENT OF X-RAY LASER MEDIA: MEASUREMENT OF GAIN AND DEVELOPMENT OF CAVITY RESONATORS FOR WAVELENGTHS NEAR 130 ANGSTROMS.		5. TYPE OF REPORT & PERIOD COVERED Final technical report 11/1/76-12/31/80
6. AUTHOR(s) Dr. James Forsyth	7. CONTRACT OR GRANT NUMBER(s) AFOSR-77-3189	
8. PERFORMING ORGANIZATION NAME AND ADDRESS Laboratory for Laser Energetics College of Engineering and Applied Science University of Rochester 250 E. River Rd., Rochester, New York 14623	9. PROGRAM ELEMENT, PROJECT, TASK AREA & WORK UNIT NUMBERS 61102F 16 2301/A7 1111	
10. CONTROLLING OFFICE NAME AND ADDRESS Air Force Office of Scientific Research Bolling Air Force Base Washington, D. C. 20332	11. REPORT DATE July 1981	
12. NUMBER OF PAGES 66	13. SECURITY CLASS. (of this report) Unclassified	
14. MONITORING AGENCY NAME & ADDRESS (if different from Controlling Office)	15. DECLASSIFICATION/DOWNGRADING SCHEDULE	
16. DISTRIBUTION STATEMENT (of this Report) Approved for public release; distribution unlimited.		
17. DISTRIBUTION STATEMENT (of the abstract entered in Block 20, if different from Report) EXCERPT AUG 3 1981		
18. SUPPLEMENTARY NOTES C		
19. KEY WORDS (Continue on reverse side if necessary and identify by block number) X-Ray, Reflectors, Laser, Plasma A		
20. ABSTRACT (Continue on reverse side if necessary and identify by block number) A new experimental facility was used to explore a range of conditions under which inverted populations on soft x-ray transitions could be produced in laser heated plasmas. Direct measurements with grating spectrographs were performed in the vicinity of 130 Å to develop the diagnostic techniques for gain determination. Designs for reflectors suitable for use in cavity resonators at soft x-ray wavelengths were developed. Construction of apparatus to produce such reflectors was begun. A patent on the reflector design was applied for.		

TABLE OF CONTENTS

Accession	NTIS	DTIC	Unannounced	Justification
Number	Code	TAB		
By		Distribution/	Availability	Codes
		Dist	Avail and/or	Special

R

Summary.....	1
Table of Contents.....	ii
I. Introduction.....	1
II. Preliminary Studies on Population Inversion in Recombining Plasmas.....	4
III. Angular Distribution of Amplified Spontaneous Emission.....	13
IV. Parameter Study of Excited State Populations in Recombining Plasmas.....	23
V. Preliminary Designs for Soft X-Ray Cavity Resonators.....	35
VI. References.....	47
Appendices	
Appendix 1 - Reprint from <u>Optics Communications</u> 24, 331-335 (1978).....	50
Appendix 2 - Abstract from "Angular Distribution of Amplified Spontaneous Emission - A Comparison of Theory and Laser Pumped Dye Amplifier Experiment".....	55
Appendix 3 - Summaries of Papers Presented at the Annual Meeting of the Optical Society of America, October, 1979.....	58
Appendix 4 - Reprint of an Abstract of New Technology.....	60
Appendix 5 - Abstract for U. S. Patent application, serial number 88,699.....	65
Acknowledgement.....	66

AIR FORCE OFFICE OF SCIENTIFIC RESEARCH (AFSC)
NOTICE OF TRANSMITTAL TO DDC

This technical report has been reviewed and is
approved for public release IAW AFR 190-12 (7b).
Distribution is unlimited.
A. D. BLOSE
Technical Information Officer

I. INTRODUCTION

The scaling laws for pumping laser devices were recognized by the earliest workers in the field to offer an enormous technological challenge to the eventual development of an x-ray laser. Indeed a practical, working device has yet to be reported in the open literature although several false or misleading reports have appeared in the past decade. One of the most promising technologies for achieving the required rate of energy delivery for x-ray laser pumping has been that of the multistage laser devices developed for the inertial confinement fusion program. We have been exploring the application of this advancing technology towards the development of a soft x-ray laser at the Laboratory for Laser Energetics for several years.

This report presents a detailed summary of several theoretical and experimental studies carried out under grant AFOSR-77-3189, "Development of Cavity Resonators for Wavelengths Near 130 Angstroms." A brief summary of the accomplishments of this study is given below.

At the beginning of this study none of the experimental tools for the construction of an x-ray laser existed. This included not only amplifying media and cavity resonators but a host of diagnostic artifacts such as bright fluorescent probe sources and beam transport optics.

Thus if one of the numerous theoretical proposals for achieving laser action at x-ray wavelength were to be verified experimentally, a straight-forward method for recognizing experimental success had to be developed. One of our first accomplishments under this grant was to model the directional characteristics of amplified spontaneous emission and to verify the predictions of this model with a free-standing, visible dye laser amplifier designed to closely replicate the anticipated characteristics of an amplifying laser produced plasma. A set of criteria for unambiguous diagnosis of the presence of gain in such an amplifier was developed.

A major accomplishment during the grant period was the experimental observation of population inversions in moderate Z, laser heated plasmas from specially configured targets. These initial observations were made using a laser which was too small to permit the experimental conditions to be scaled to a geometry which would permit direct verification of gain. However, a systematic parameter study of the factors which significantly affect the observations was initiated. These studies are in active pursuit at present. Also, during the grant period the Laboratory for Laser Energetics (LLE) acquired major new laser facilities which have become available for this work. We believe these facilities will enable us to attempt a direct measurement of gain in the soft x-ray region.

The prospect of successfully achieving soft x-ray amplification has motivated us to consider the question of a suitable strategy for the eventual construction of a soft x-ray cavity resonator. Under the grant we have undertaken a program of extensive modelling of the possible performance characteristics of periodic, multilayer, thin film structures in this application. One result of this study was a new design which permits the use of discrete length polymer chains in a Langmuir-Blodgett structure while allowing the wavelength of peak reflectance to be tuned to a particular (i.e. arbitrary) wavelength. A patent application has been filed on this design.

During the past four years great progress has been made toward the construction of a practical soft x-ray laser. A candidate amplifying medium has been experimentally identified and a procedure to diagnose its performance has been developed. The probable performance of realizable cavity resonator structures is under study and such structures should provide adequate feedback under anticipated experimental conditions. Definitive experiments on soft x-ray laser action should be possible in the near future as a consequence of these studies.

II. Preliminary Studies on Population Inversions in Recombining Plasmas

When very intense pulses from a laser are focused onto solid targets, a hot high density plasma is formed near the solid surface. The incident laser energy is deposited primarily near the critical density region of the plasma, i.e. the region where the plasma oscillation frequency is equal to the incident laser frequency. For a Nd^{+3} :glass laser ($\lambda=1.054\mu$) the critical electron density has a value of 10^{21} cm^{-3} . Modern multistage glass laser systems producing terawatt level pulses of subnanosecond duration can achieve focused intensities exceeding 10^{16} W/cm^2 and will produce plasma electron temperatures of 1Kev in the critical density region. Such plasmas are composed predominantly of highly stripped ions.

As the plasma expands away from the solid surface, the particle temperatures drop rapidly and recombination takes place. The two principal recombination processes occurring in the underdense region of the plasma are radiative recombination (the inverse of photoionization) and three-body recombination (the inverse of collisional ionization). It is well known that in recombining hydrogen-like and helium-like plasmas, radiative recombination favors the population of low lying principal quantum levels while three-body recombination is favored into high lying levels. Gudzenko and Shelepin first pointed out that inverted populations would be possible in recombining plasmas under conditions where three-body recombination would predominate.¹ Numerous theoretical treatments of these conditions have subsequently been given², and several reports of measured population inversions in expanding, laser produced plasmas

have appeared.³ Until recently,⁴ however, none of the estimated inversion densities reported has been high enough to represent useful gain or to attempt direct demonstration of laser action.

If one compares the ratio of collisional to radiative recombination rates in hydrogen like plasmas⁵, one finds that for a given ratio of ion excited state energy to electron temperature, the electron density required for the dominance of collisional recombination scales as Z^3 . Thus, provided one can excite high Z plasmas to nearly full ionized conditions, one has much higher electron densities at which inversion conditions would be favored. The corresponding population inversion densities will be higher as well. In our experiments we employed a laser of much higher power than that employed by previous workers enabling us to excite aluminum targets to the appropriate level of ionization. Previous workers were able to employ only carbon plasma. We observed population inversion at 10-1000 times higher electron density than previously observed.

One problem which develops at high particle densities is that collisional recombination may occur very rapidly, before the plasma has had time to expand, cool, and insure depopulation of the lower lying states. To provide for adequate cooling in our experiments a stepped target design was employed to provide a high density heat sink in the expanding plasma.

Our experimental arrangement is shown in Figure 1. A multistage mode-locked Nd^{+3} :glass laser was employed producing single 200 psec pulses with up to 10J in energy. The laser pulses were focused on the aluminum target surface by an f/3.5 aspheric lens so that the edge of

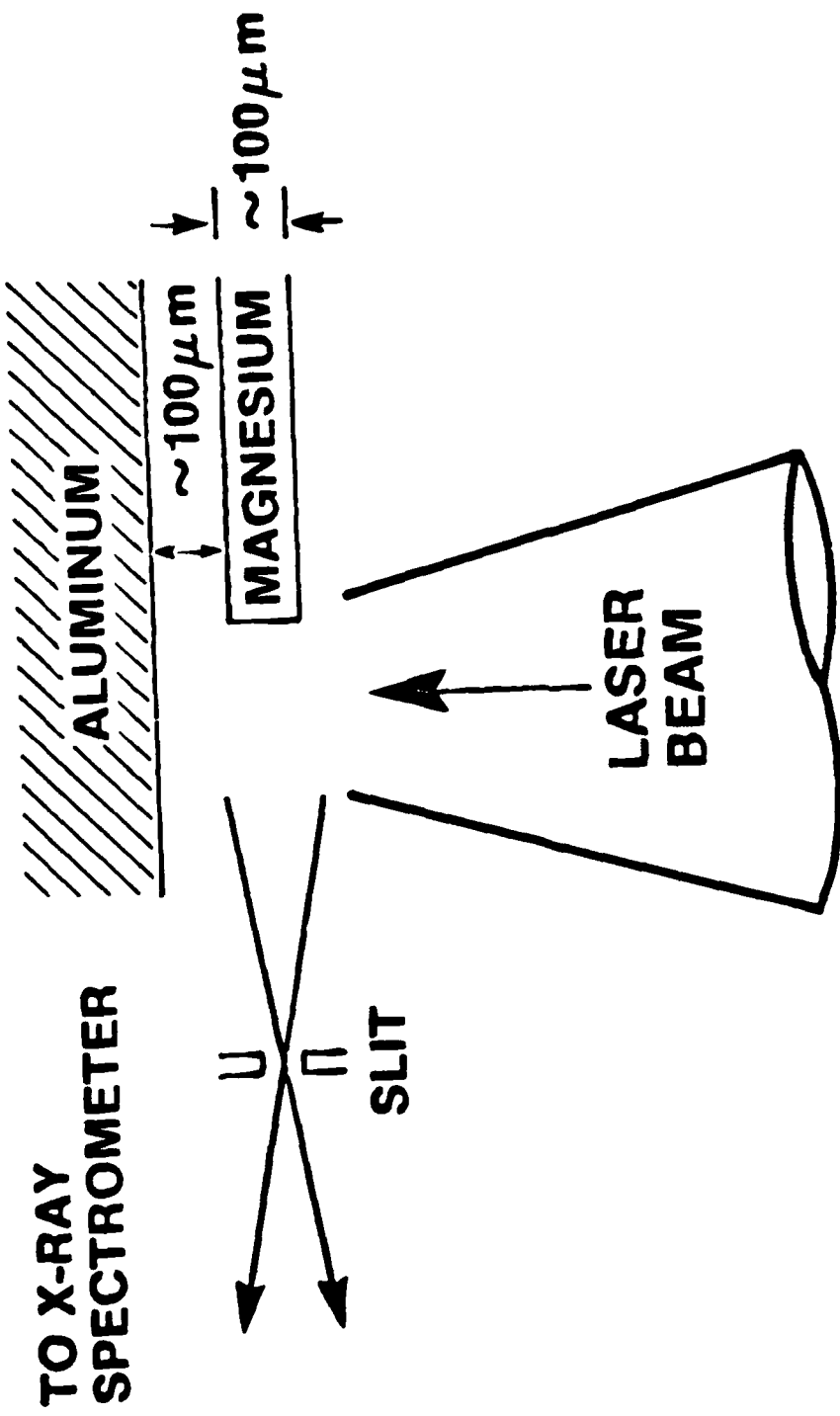


Figure 1

the focused beam grazed a thin magnesium plate set slightly in front of the aluminum block. A spatially resolving crystal spectrograph was located near the target surface and oriented to record the radiation from the expanding plasma. The spatial dispersion was arranged along the direction normal to the target surface. The spectrograph recorded emission lines from the plasma in the wavelength range of $6-8\text{\AA}$, corresponding to radiative transitions from the various principal quantum levels of Al^{+11} and Al^{+12} to the respective ground states. In the underdense regions of the expanding plasma, collisional depopulation of the excited states is negligible compared to radiative decay. Thus the intensities of the emission lines are a direct measure of the level populations.

In Figure 2, two spectra obtained from the instrument described above are shown. These spectra were recorded on the same single shot but were produced by emitting regions at different distances from the target surface. The upper trace shows the emission spectrum near the target surface. The regular decrease in the line intensities as a function of principal quantum number in the two ion species is normal for high density high temperature plasmas. In the lower spectrum, recorded from a region approximately $400\text{ }\mu\text{m}$ from the target surface, a distinct reversal of this trend is evident in the helium-like series. An unambiguous inversion in emission intensity, and thus in population, between the $1s4p$ and $1s3p$ levels is evident. A complete examination of such spectra shows that in the geometry employed here, population inversion between these levels begins approximately $150\text{ }\mu\text{m}$ from the target surface, reaching its maximum density approximately $350\text{ }\mu\text{m}$ from the surface.

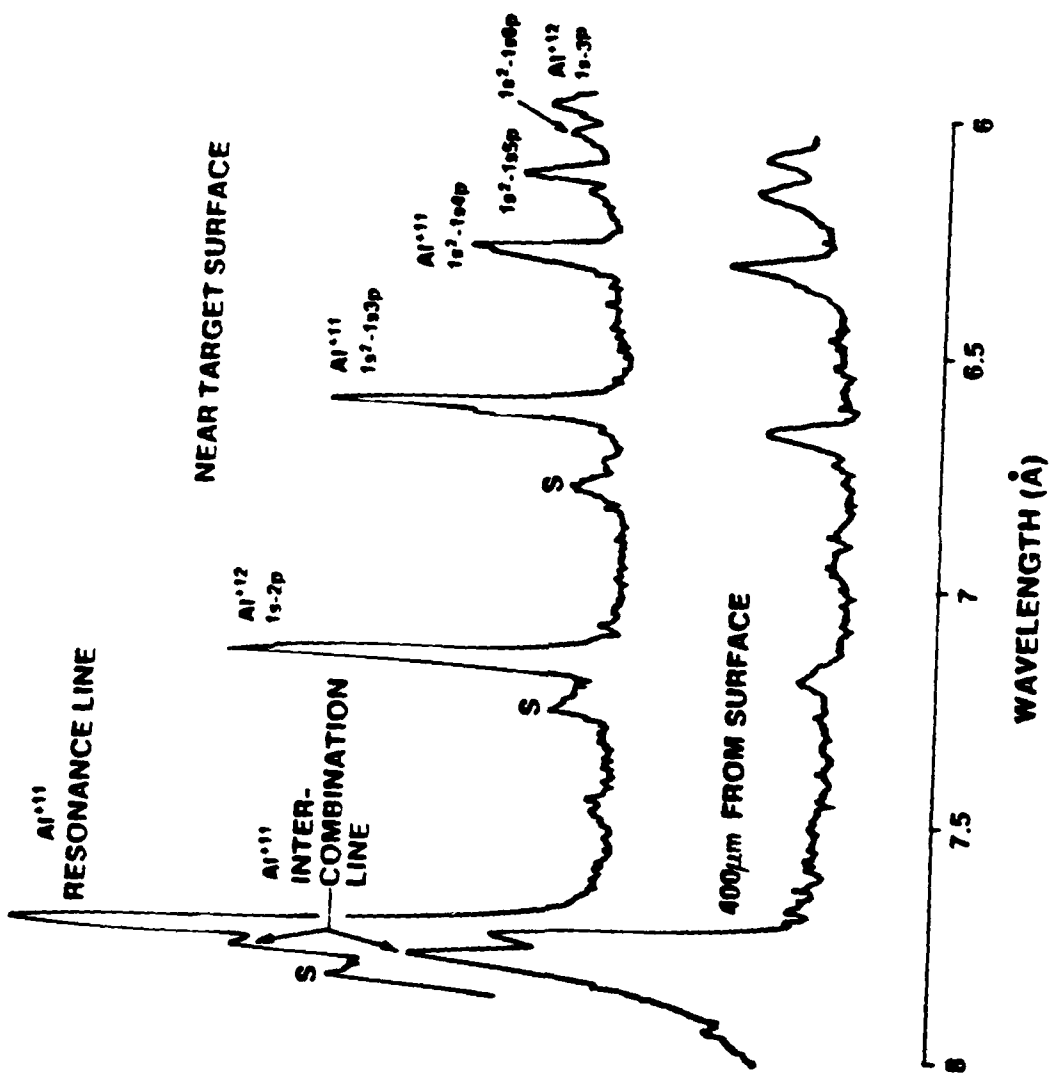


Figure 2

The experimental results have been compared to numerical calculations with the one dimensional two-temperature hydrodynamic code SUPER which includes rate equations for the evolution of the aluminum ion charge states and excited level populations and an escape factor approximation for line radiation transport.⁶ A comparison of the computed and measured spatial electron temperature distribution is shown in Figure 3. The measured electron temperatures were obtained from the intensity ratios of the resonance lines of the hydrogen-like to the helium-like ions.⁷ A comparison of the measured and computed electron density distributions along with the distribution of population inversion density is given in Figure 4. The electron density was measured from the intensity ratio of the resonance line to the intercombination line in the helium-like ion.⁸ The effect of the heat sink was included in the numerical model by assuming a lateral temperature gradient scale length of 200 μm , conducting heat into a sink of electron density 10^{21} cm^{-3} at a location corresponding to the magnesium plate. The generally close agreement obtained gives us confidence that the numerical model may be used to help us further optimize the experimental conditions for population inversion.

Having demonstrated an inverted population in the plasma, we turn our attention to the potential amplifying properties of the medium. We estimate the gain coefficient for the $4\ ^3\text{F} - 3\ ^3\text{D}$ manifold⁹ at 129.7\AA to be of the order of 10 cm^{-1} . Using a circular focal spot geometry the measured plasma width in the inversion region is approximately 200 μm . The gain length product is of the order of 0.2 corresponding to a single pass gain of 22%. Although significant by visible laser standards, this is too low to measure directly at soft x-ray wavelengths.

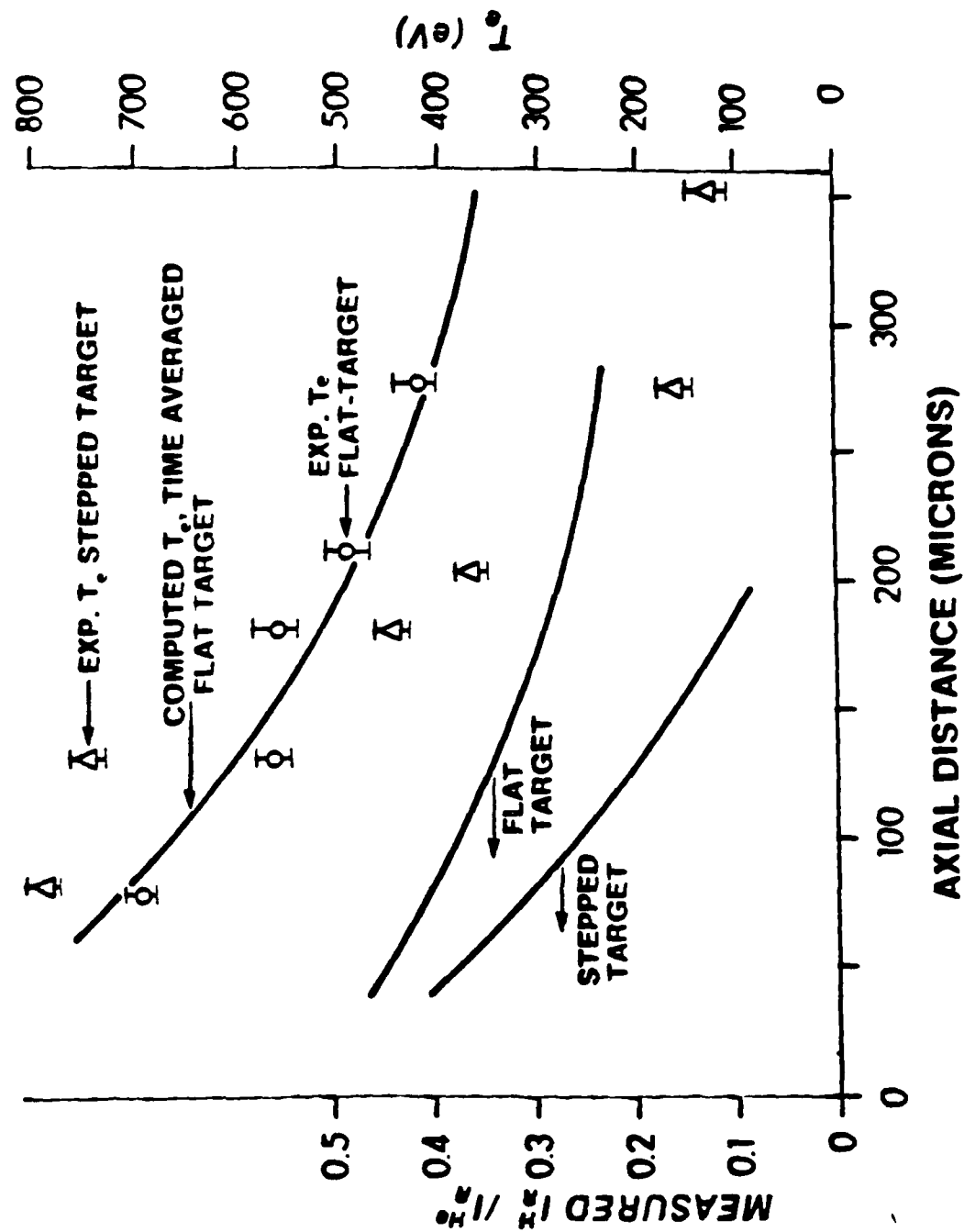


Figure 3

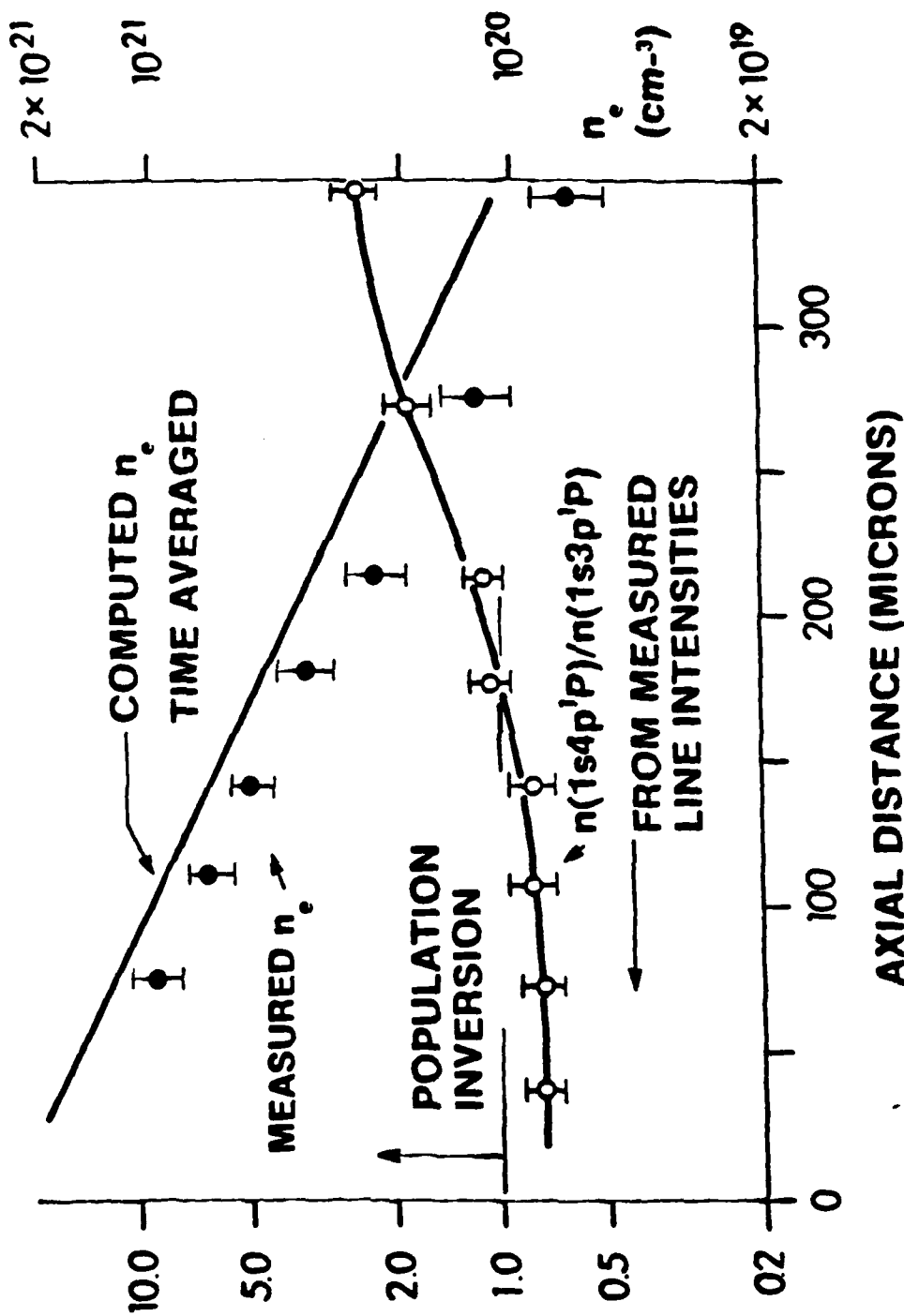


Figure 4

In the experiments performed to date, a maximum laser pulse power of 50 GW was employed, focused into a circular spot of approximately 60μ in diameter. In order to extend the present work to a line focus geometry, higher laser power is required. This is because the irradiated area of the target is larger, and we wish to maintain the target illumination intensity in order to achieve the appropriate plasma particle temperatures required to reach the necessary ionization stages. A single beam $\text{Nd}^{+3}:\text{glass}$ laser is available at LLE, delivering in excess of 500 GW in single pulses. Preliminary tests on our target interaction apparatus indicate that the focal spot size of this beam is well below 50 μm , possibly as small as 20 μm . This improved focusability is consistent with the design goals and the measured beam divergence of this facility. Thus it appears that we should be able to reproduce our previous experimental conditions in line focus geometries up to a few millimeters in length. It seems quite likely that an overall single pass gain of 10 could be achieved in this way.

III. Angular Distribution of Amplified Spontaneous Emission

A principal objective of our research is to develop soft x-ray amplifying media with sufficient gain to serve as the basis for a practical laser amplifier or oscillator. Detection of the presence of an inverted population is a necessary, but not sufficient step toward meeting this objective. We have, therefore, made a study of methods of diagnosing the presence of gain in a medium whose characteristics are transient and not perfectly reproducible. This study has been carried out using both analytic modelling and experimental measurements on a dye amplifier. In this section we present a brief summary of the salient features of this study. The detailed results of the study are attached at the end of this report. This work was submitted in partial fulfillment of the requirements for the Ph.D. degree at the University of Rochester.¹⁰

We describe the amplification of the radiation field in the amplifier by a steady-state, geometric (no diffraction) radiation transport equation. The transport equation is

$$\bar{s} \cdot \nabla I_\nu(\bar{s}, \bar{x}) = [N_b(\bar{x}, \nu) \sigma_{ba}(\nu) - N_a(\bar{x}, \nu) \sigma_{ab}(\nu)] I_\nu(\bar{s}, \bar{x}) + N_b(\bar{x}, \nu) \sigma_{ba}(\nu) \frac{2h\nu^3}{c^2}$$

where $I_\nu(\bar{s}, \bar{x})$ is the specific intensity or spectral radiance at a point \bar{x} in the medium in the direction \bar{s} at a frequency ν .¹¹ $I_\nu(\bar{s}, \bar{x})$ has units of power per unit area per steradian per unit frequency interval. Because the propagation time in the medium is assumed to be small compared to the temporal variations, the time dependence of $I_\nu(\bar{s}, \bar{x})$ may be considered explicitly. $N_b(\bar{x}, \nu)$ and $N_a(\bar{x}, \nu)$ are the population densities of the upper and lower laser levels, respectively, and in general are

functions of position and frequency. $\sigma_b(v)$ and $\sigma_a(v)$ are the stimulated emission and absorption cross-sections and are also functions of frequency.

Two contributions to the increase in spectral radiance are considered: net stimulated emission and fluorescence. The net stimulated emission is the difference in stimulated emission, $N_b \sigma_{ba} I_v$, and absorption $N_a \sigma_{ab} I_v$. Fluorescence or spontaneous emission, $N_b \sigma_{ba} \frac{2hv^3}{c^2}$, is often neglected in laser oscillator calculations; however, fluorescence must be included in ASE calculations because it is the sole source term. The medium is assumed to be optically thin so that resonant absorption (and thus radiation trapping) and scattering may be neglected.

We have considered the solution to the radiation transport equation for two kinds of amplifier geometry. In one case we consider a rectangular medium of square cross section with a spatially uniform distribution of gain. The radiation transport characteristics are considered for various geometrical aspect ratios and gain-length products. In the second case we consider a rectangular medium divided into two zones: one zone exhibits gain uniformly within the zone, while the other zone exhibits strong fluorescence but no amplification. This second case is intended to model a laser plasma in which soft x-ray amplification may be present in only the lower density regions. This would be the case with the recombination scheme described earlier.

The laser-pumped dye amplifier experiment was designed to simulate an optically freestanding ASE source or amplifier with a non-uniform transverse gain profile. Our objective was to measure the ASE angular distribution and to compare the observed dependence of the distribution on the gain coefficient and the amplifier geometry to that predicted by the ASE theory.

The experimental set-up for the dye amplifier ASE experiment is shown schematically in Figure 5. R6G dye in an index matched quartz dye cell was optically pumped by a 15 nsec pulse from a frequency doubled, $\text{Nd}^{+3}:\text{Yag}$ oscillator and glass laser amplifier system. The angular distribution of ASE from the dye was measured at discrete angles using silicon photodiodes, and continuously about the longitudinal axis using Tri-X film. The pumped length of the dye cell was varied using an aperture, thus permitting a gain measurement independent of the angular distribution measurements.

Scale drawings of two experimental table configurations are shown in Figures 6 and 7. The entire table was covered by a flat black light-tight box to block both amplifier flashlamp light and room light. Two 45° dielectric mirrors with R_{\max} at 532nm were used to align the pump beam on the experimental table and into the dye cell. These mirrors also filtered out the unconverted 1.06μ beam.

The pump beam was vertically focused by a positive cylindrical lens (creating a horizontal line focus) and then expanded by a negative spherical lens as shown in Figure 8. This lens configuration produced a diverging beam with an elliptical cross-section; at the dye cell the horizontal magnification was eight while the vertical magnification was approximately 1.6. The central portion passed through a rectangular aperture to control the distribution of pump light to the dye. Half of the pump beam (away from the detectors) was blocked by the aperture for one-half length amplifier shots.

Pump beam alignment was facilitated by using a coincident beam from a HeNe laser to center the beam through the dye cell and to ensure proper beam focusing. The final alignment was obtained by

ASE LASER PUMPED DYE EXPERIMENT

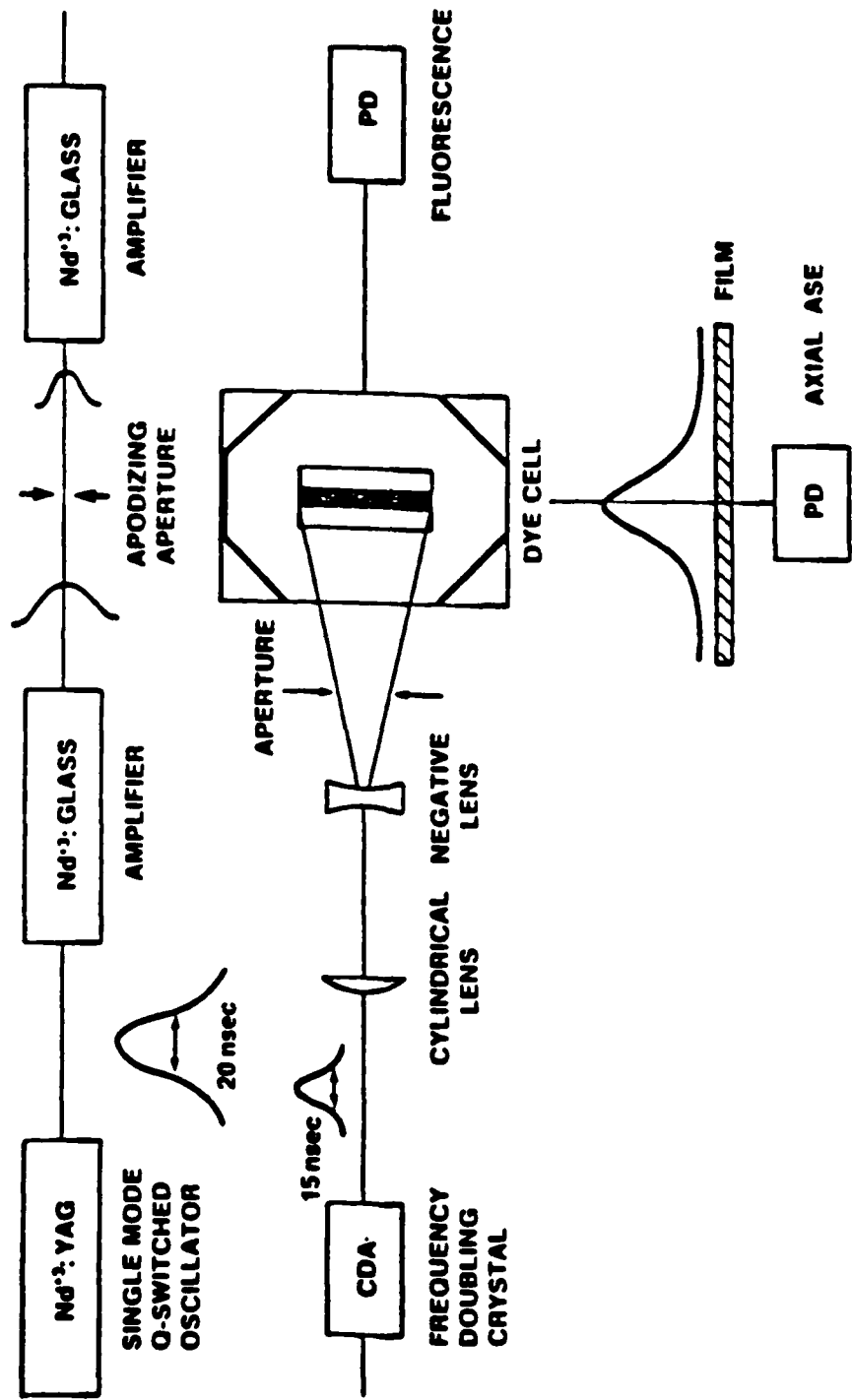


Figure 5

SET UP DYE AMPLIFIER EXPERIMENT

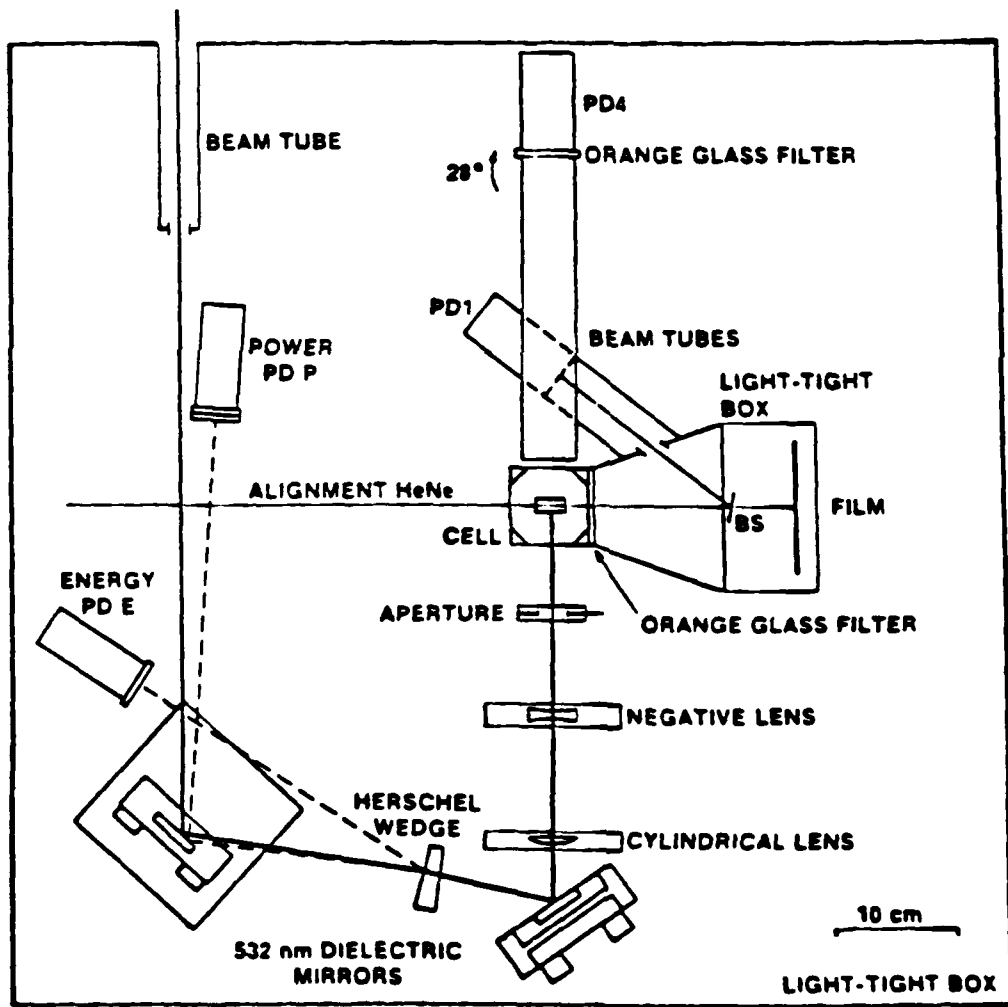


Figure 6

SET UP DYE AMPLIFIER EXPERIMENT

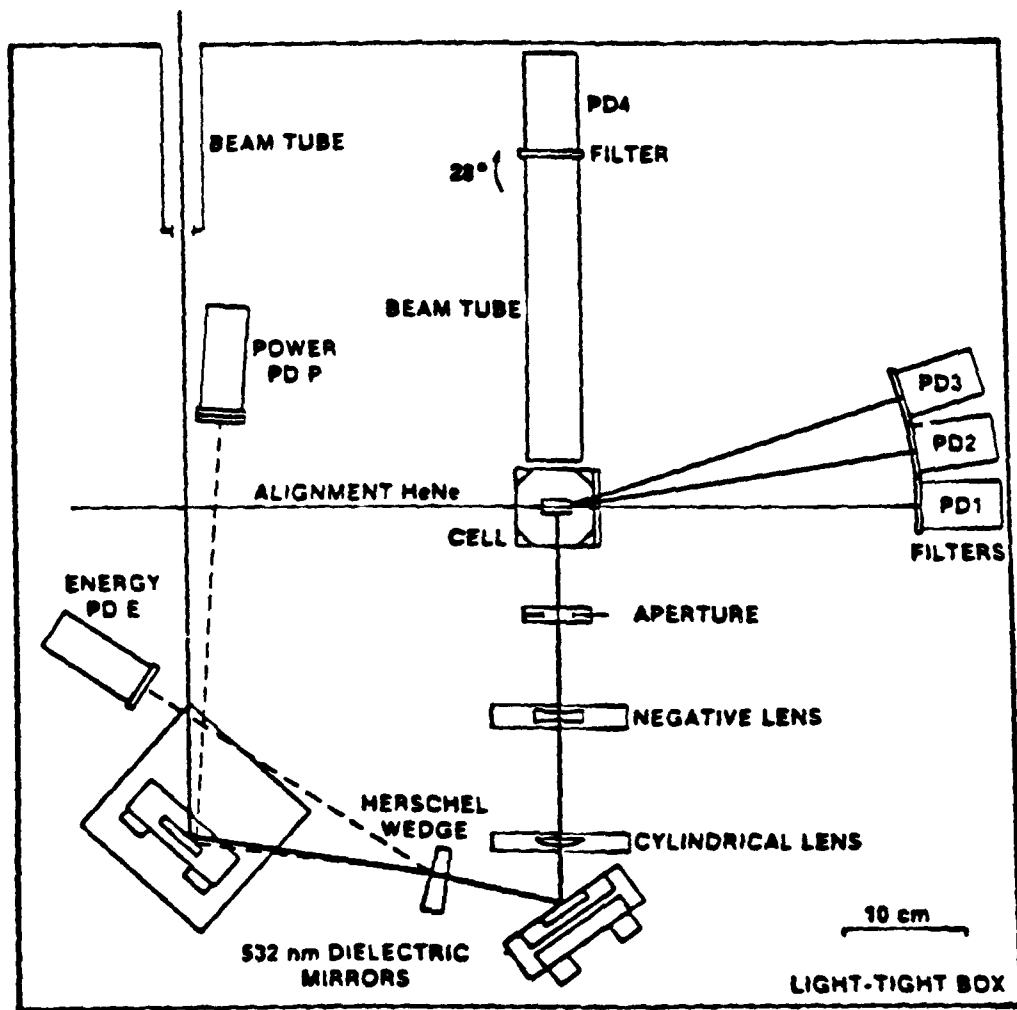
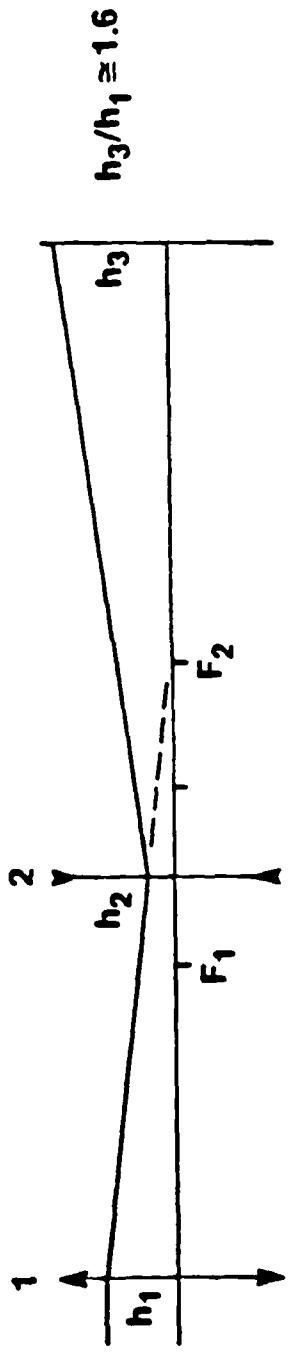


Figure 7

FOCUSING GEOMETRY

SIDE VIEW



CYLINDRICAL
LENS

$$F_1 = 17\text{cm}$$

NEGATIVE
LENS

$$F_2 = 2.5\text{cm}$$

DYE
CELL

TOP VIEW

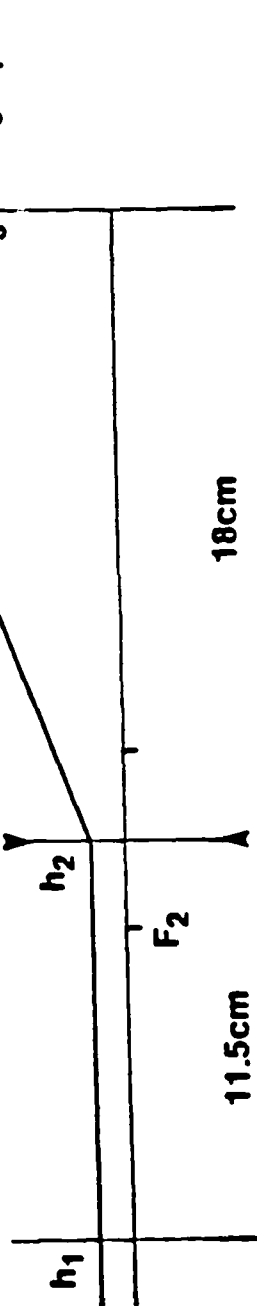


Figure 8

photographing the beam transmitted through the dye cell on Polaroid 410 film using only the frequency doubled oscillator pulse. This also provided a qualitative estimate of the pump beam uniformity. For a typical pump beam profile, approximately 35% non-uniformity was obtained.

A Herschel wedge was inserted in the pump beam to reflect approximately 4% of the beam to each photodiode, PDE and PDP. PDE measured the pump beam energy and was calibrated using a Gentec calorimeter. PDP monitored the pump beam temporal profile. A fraction of this energy (due to beam expansion and obscuration of the beam) pumped the dye.

The R6G fluorescence power was temporally resolved by PD4. PD4 was located perpendicular to the dye cell axis and 28° above the horizontal plane. This orientation, combined with a beam tube and a 560nm cut-off, long-pass orange glass filter, prevented significant pick up of the green pump beam. PD4 was sufficiently distant from the cell (29cm) for the fluorescence to be isotropic over the collection angle.

The ASE along the dye cell axis was time resolved by PD1 as shown in Figure 6. A small beamsplitter (1cm square) directed 25% of the axial ASE to PD1. PD alignment was obtained using a HeNe beam centered along the dye cell bore. Pump light was excluded by the use of a beam tube and an orange glass filter.

The temporally integrated angular distribution was measured simultaneously using 4"x5" panachromatic Tri-X film located behind the beam-splitter in a standard film holder. A black cardboard light box connected the film holder and dye cell, preventing stray light from fogging the film.

A second configuration is shown in Figure 7 in which the ASE was measured along the dye cell axis by PD1 and in the horizontal plane by PD2 and PD3. Orange glass filters: 560nm cut-off, long-pass, were used on the PD's.

We find good agreement between the analytic model and the experimental measurements over the range of geometries and gain coefficients investigated. It is found that in high aspect ratio, i.e. needle-shaped, amplifying media that the angular distribution of the radiation is the most sensitive practical diagnostic of the presence of gain. It appears that a gain length product of unity may be diagnosed under favorable conditions; under pessimistic conditions a gain length product no greater than three may still be adequate.

While the directional characteristics of an ASE source of this type would be interesting, such a level of amplification would make the construction of a feedback device an intriguing possibility. Of course, the normal incidence reflectivity of solid materials is very low for all wavelengths shorter than 300 \AA due to severe photoelectric scattering. However, it is possible to design periodic structures consisting of alternating layers of high Z and low Z materials which might be expected to exhibit significant reflectivity in this wavelength range.¹²⁻¹⁴ Attempts to produce such structures by evaporative deposition have been largely unsuccessful due to the intrinsically stringent controls needed on film thickness.¹³ Accordingly, we have considered various non-evaporative deposition methods, especially the use of Langmuir-Blodgett layers¹⁵ of insoluble fatty acids. During the course of these investigations we received a very interesting suggestion from Professor Henke.¹⁶

He pointed out that multilayer structures of this type¹⁷ have an energy resolution of the order of 1ev, i.e. a resolution of 1 \AA in the vicinity of 120 \AA . He also pointed out that lead lignocerate has a 2d periodicity of 130 \AA . Therefore, such a multilayer should exhibit significant normal incidence reflectivity at a wavelength of 129.7 \AA , the calculated wavelength of our amplifying transition. We have subsequently calculated a normal incidence reflectivity of 11% for such a structure. Accordingly, as part of our program we propose to examine such structures further as this is sufficient reflectivity to produce oscillation at gain levels estimated earlier.

IV. Parameter Study of Excited State Populations in Recombining Plasmas

Since our initial measurements described in Section II were made, our experimental apparatus was installed in a laboratory located to receive pulses produced by LLE's Glass Development Laser (GDL). This laser was built as an engineering prototype of LLE's 24 beam OMEGA laser system. The prototype studies were completed in 1978 and the GDL system is now being used to perform a variety of scientific experiments, including the soft x-ray laser development experiments to be described. The GDL system is rated at 500 GW pulse power in 50 psec FWHM pulses and up to 160 joules per pulse in 1 nsec FWHM pulses. The pulse repetition rate is 2 shots per hour, the highest of any high power glass laser system in operation or under construction. A beam divergence of 100 μ rad or better is measured at full rated output. This corresponds to near diffraction limited performance at the output aperture of 9 cm and is achieved by extensive use of spatial filters in the laser amplifier chain. A schematic diagram of the GDL system is given in Figure 9.

The GDL system is equipped with two mode-locked oscillators, one optimized for short pulse (e.g., 50 psec) production and the other optimized for long pulse (e.g., 500 psec) production. This enables rapid changeover in system pulselwidth to efficiently fill the requirement of the several experimental facilities served by the GDL laser system.

The spatially resolved crystal spectrograph experiments described above were repeated using the GDL laser system at 150 psec, 400 psec, and 700 psec FWHM pulses. The results obtained are quite similar to that shown in Figure 10 and show little dependence on laser pulselwidth.

GDL SYSTEM LAYOUT

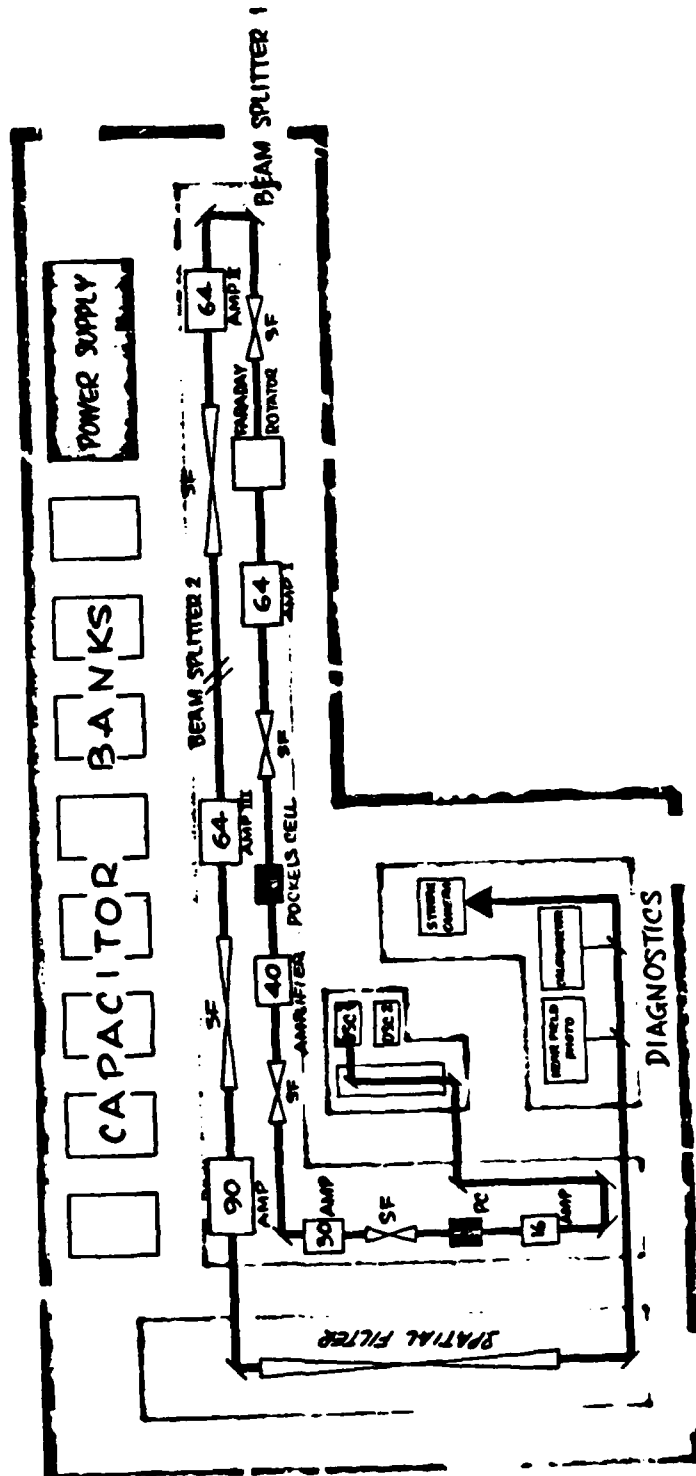


Figure 9

EVIDENCE FOR POPULATION INVERSION OF THE $n=3,4$ LEVELS OF
 Al^{+11} AT $400 \mu\text{m}$ FROM THE TARGET

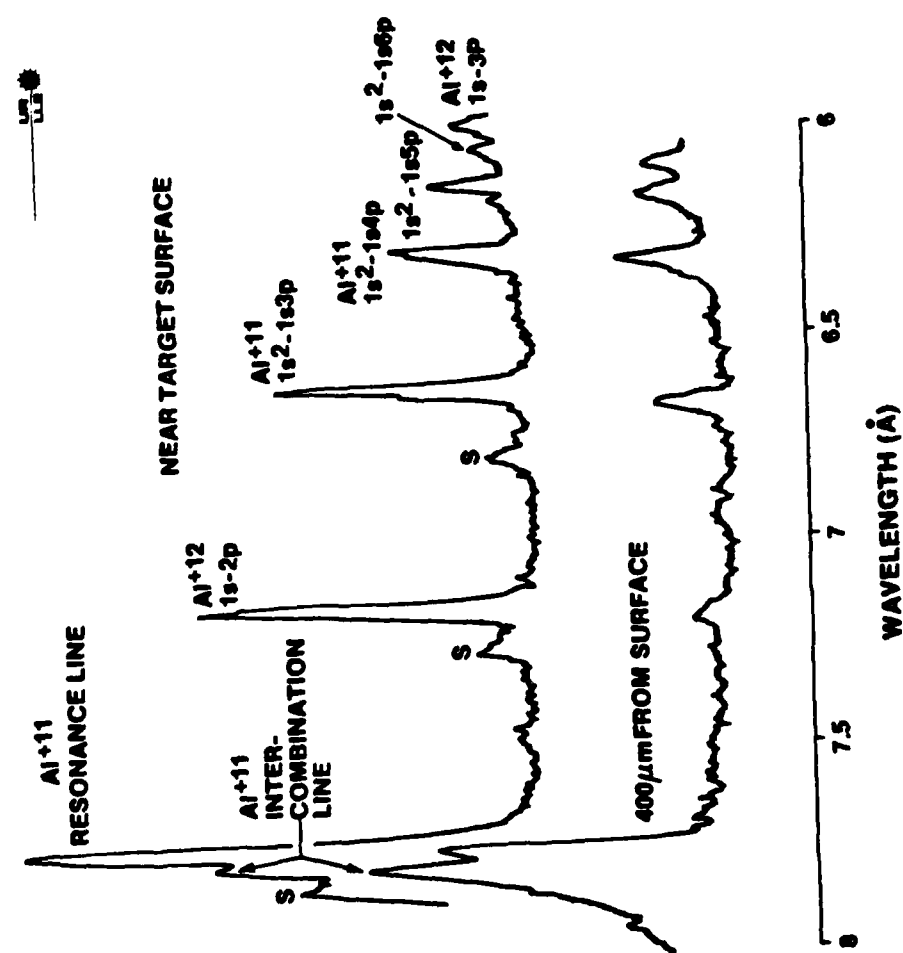


Figure 10

This suggests that the plasma expansion from the solid surface may be characterized by a kind of stationary flow in this geometry and that the heat sink has more than a transient effect on the temperature profile in the expansion region. Further experiments were conducted to determine the characteristics of the heat sink.

To learn more about the transport of energy from the plasma to the heat sink the geometry shown in Figure 11 was modified by adding a second heat sink element in the plane of the first, but with its edge on the other side of the core of focused rays from the laser pulse. This results in a heat sink geometry in the form of a slit. The orientation of the heat sink slit was chosen to allow the spatially resolving crystal spectrograph to view along the slit opening, perpendicular to the view illustrated in Figure 11.

A spatially resolved spectrogram is shown in Figure 12 which illustrates both the experimental technique and the operation of the heat sink. In this experiment a 58 joule 400 psec FWHM laser pulse was focused on the surface of an aluminum target to a focal spot diameter of approximately 100 μm . The heat sink slit was constructed of lead foil and was located 100 μm from the target surface and had an opening of approximately 200 μm . The spectrograph slit was oriented with its opening in the plane of incidence of the flat diffracting crystal providing spatial resolution normal to the surface of the target. The slit was adjusted to give a spatial resolution of approximately 50 μm .

EXPERIMENTAL CONFIGURATION FOR MEASURING
POPULATION INVERSION

U.S.
U.S.
U.S.

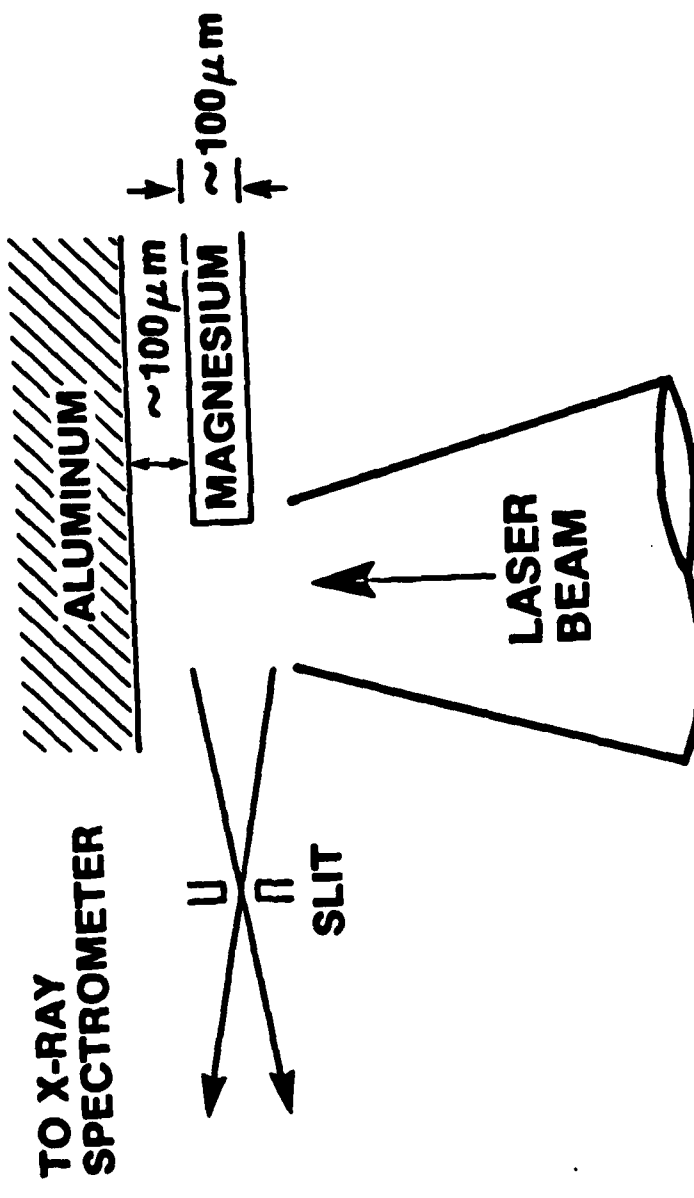
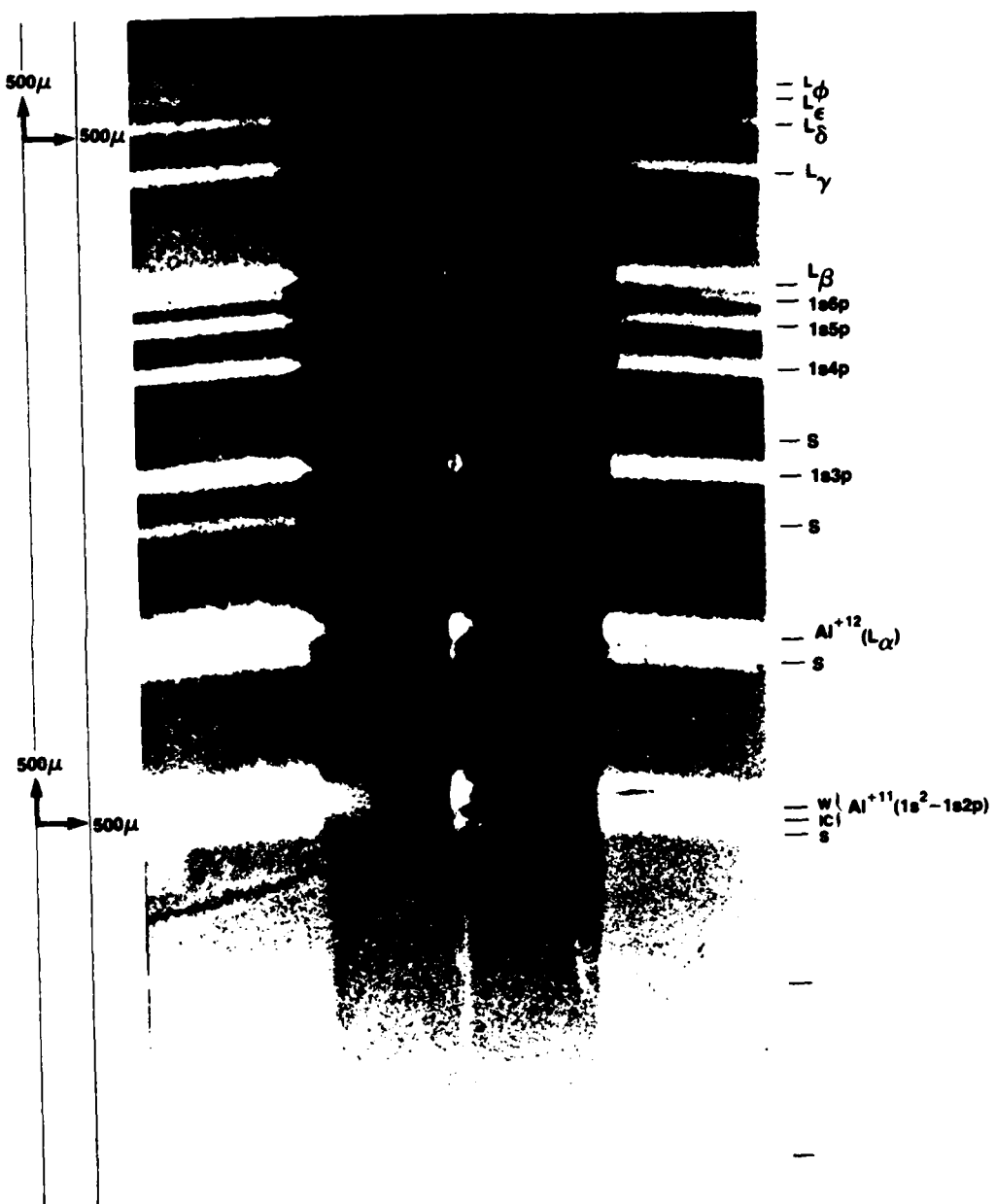


Figure 11



shot #960
 58.1 Joules—400 psec
 target: Al+Pb (silt)

X140

Figure 12

When the spectral components of the source are well separated in the spectrograph, as is the case here, the observed widths of the lines will be determined by the spatial extent of the source unless a second slit is included in the spectrograph with its opening normal to the plane of diffraction. We deliberately omit the second slit in order to obtain spatial resolution of the source parallel to the surface of the target, in this case of the order of $40 \mu\text{m}$. In effect, then, we have two dimensional spatial resolution of the emission of each of the principal emission lines from aluminum ions in the range of $5 - 8\text{\AA}$.

The spatial resolution slit is constructed out of two small steel pins which allow some radiation to pass directly to the crystal on either side of the pins. The spectra recorded here are spatially integrated in the direction normal to the target. The spatial integration is complete outside the shadow of the pins. However, the shadow of the pin farthest from the target surface will be partially illuminated by radiation from the expanding plasma. This shadowgram spectrum is partially spatially integrated and is increasingly localized into the shadow.

In Figure 12 we see fully integrated spectra displayed vertically on the right- and left-hand side of the figure. The shadowgram spectrum is visible in the left-hand shadow which the fully spatially resolved spectrum appears in the center. In this geometry the image magnification varies slightly along the direction of spectral dispersion so a spatial scale has been included on the left side of the figure. Identification of the hydrogen-like (Lyman) transitions and of the upper levels corresponding to transitions to the ground state in the helium-

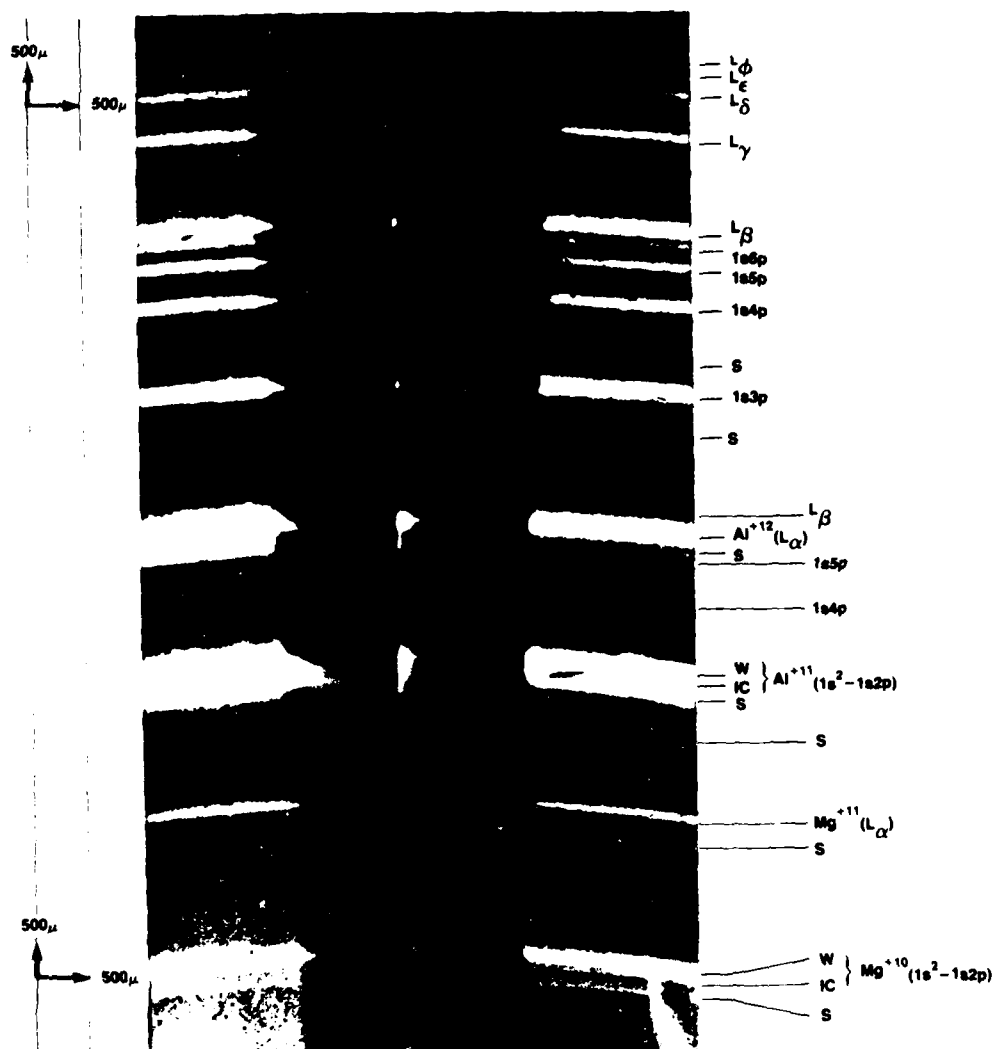
like ions of aluminum is given on the right hand side of the figure. The target surface position in the spatially resolved spectra is at the left side portion of each spectrum with the plasma expanding toward the right.

Several interesting features are apparent in the spatially resolved spectrum in Figure 12. Each line in the spectrum exhibits bright emission near the target surface, the hot, high density region of the plasma. The emission drops abruptly due to the gradual decrease in both temperature and density in the expanding plasma until it strikes the heat sink. At this point the emission increases dramatically, particularly in the higher series lines from the helium-like ions where the emission becomes brighter than it was at the target surface. This is consistent with an enhanced degree of collisional recombination, due to a sudden local temperature drop, which favors population of the higher quantum levels of an atom. It appears that the instantaneous effect of the heat sink is quite localized and is produced by collision of plasma ions with the heat sink surface, rather than due to a pre-plasma produced from the heat sink by the edges of the laser beam. As the aluminum plasma expands beyond the heat sink, lateral thermal conduction cools the central portion of the jet and the emission lines persist for several hundred microns or more, particularly from the higher lying series members. (This persistence is better exhibited on the microdensitometer traces in Figure 10 than in the spectrogram reproduction in Figure 12.)

With this spatially resolved spectroscopic technique we may now begin to address the question of the optimization of the heat sink construction. The results of an experiment to test the effect of heat sink composition is shown in Figure 13. The target irradiation conditions were similar to those used to obtain Figure 12 except that the heat sink was composed of two different metals. With reference to the figure the upper edge of the heat sink was made of a magnesium foil which the lower edge was made of lead foil. With reference to the emission in the plane of the heat sink there is no clear difference in the effectiveness of the two materials even though they have quite different thermal conductivities and heat capacities.

It is interesting to observe the appearance of magnesium lines in this spectrum. The emission begins at the heat sink surface and moves outward, away from the target surface. This is consistent with collisional heating and momentum transfer from the expanding aluminum plasma. If the heat sink were being ionized by the edge of the laser pulse one might expect some motion of the magnesium ions toward the target surface as well.

Since the observation of inverted populations appears to be straightforward with our technique, and since it does not appear to critically depend upon the various experimental parameters, we have now turned our attention to direct measurements of the emission from the various excited state transitions of helium-like aluminum in the range from 50 to 400 Å. These measurements are being made with a grazing incidence grating spectrograph.



shot #978
 54.3 Joules—400 psec
 target: Al + { Mg (up)
 Pb (down)}

x136

Al | Mg

Figure 13

Our first tests with this spectrograph have just been completed at this writing. Our spectrograph was fitted with a 40 cm radius, 600 grove/mm platinum coated grating with a blaze angle of $1^{\circ} 35'$. The entrance slit was 20 μm wide for these first tests and located approximately 10 cm from the laser plasma. The spectrograph was fitted with a spatially resolving slit approximately 100 μm wide; the spectrograph viewing direction was along the target surface so the emission was spatially resolved in the direction of plasma expansion.

A microdensitometer trace of one portion of a grating spectrum is shown in Figure 14. This recording was obtained from a single 87.7 joule 700 psec FWHM laser pulse. The wavelength scale is only approximate and we are just beginning the task of identifying the prominent spectral components in the recording. At this juncture the important point is that we have demonstrated single shot recording capability in this spectral region and are prepared to begin a systematic investigation to discover radiation transport effects in line focus geometry associated with an amplifying condition.¹⁸

SPECTRUM 100μ AFTER THE MAGNESIUM FOIL

I - Normal to the line focus (shot #325: 97.7J, 700 psec)
II - Along the line focus (shot #331: 80.5J, 700 psec)

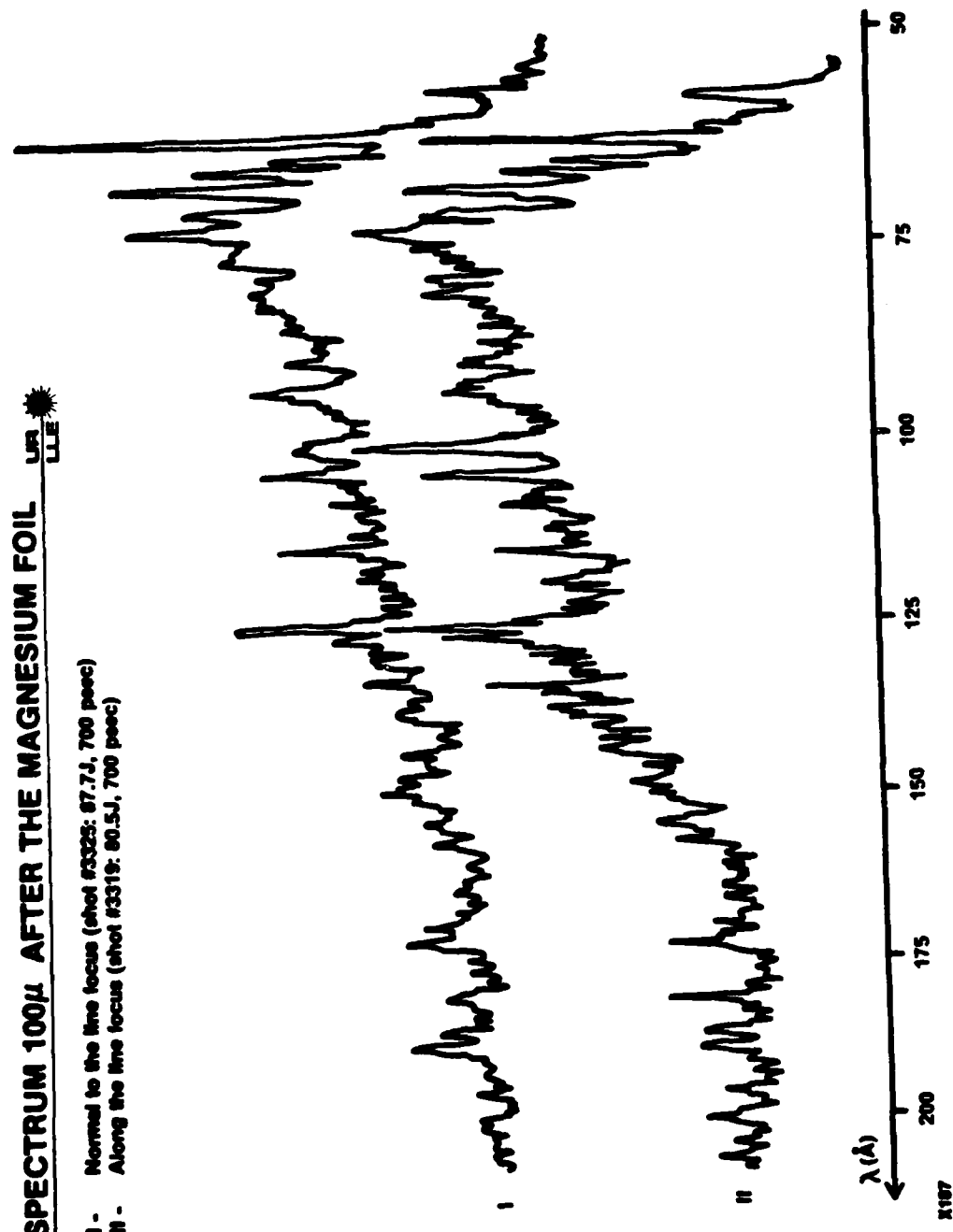


Figure 14

V. Preliminary Designs for Soft X-Ray Cavity Resonators

In this section we describe a mirror structure that can provide a high normal incidence reflectivity at any chosen soft x-ray wavelength in the range $70 \text{ \AA} - 300 \text{ \AA}$, where conventional metallic reflectors cannot function. The new reflector is a modified multiple bilayer structure consisting of a periodic array of fatty acid films separated by thin metallic layers. Schematic enlargements of typical structures are shown in Figs. 15 and 16.

Principles of Operation

At wavelengths shorter than 300\AA , ordinary disordered solid materials have very weak normal incidence reflectances since their indices of refraction approach closely to unity. Similarly, a weak reflection may be obtained at each boundary in a periodic structure of the sort formed when layers of high and low density material are deposited alternately. If the period length of the structure is set to the correct value, which will be near but not precisely equal to half the wavelength of the normally incident radiation, the reflected components from the various boundaries will combine constructively to yield a strong overall reflection.

A well-known class of structures that satisfy the above conditions at certain wavelengths in the range $70\text{\AA} - 160\text{\AA}$ are the Langmuir-Blodgett multilayers. Such a structure is formed by floating a monomolecular fatty acid film on a heavy metal ion solution and then attaching the monolayer to a mirror substrate by dipping the substrate into the solution (Figure 17). A layer is deposited on each downstroke and sometimes

USE OF MIXED SPACINGS TO MATCH MIRROR RESONANCE TO SOURCE WAVELENGTH

UR
LLE

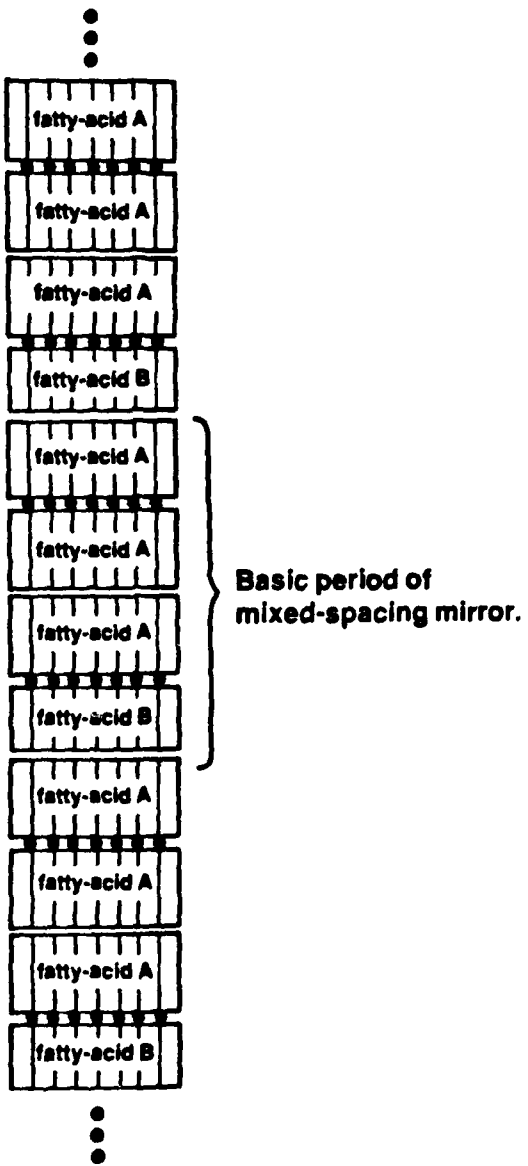
In this example:

$$N_A = 3N_B$$

Then:

$$\lambda_{PEAK} \approx \frac{3}{4}2d_A + \frac{1}{4}2d_B$$

(for $2d_A - 2d_B$ small)

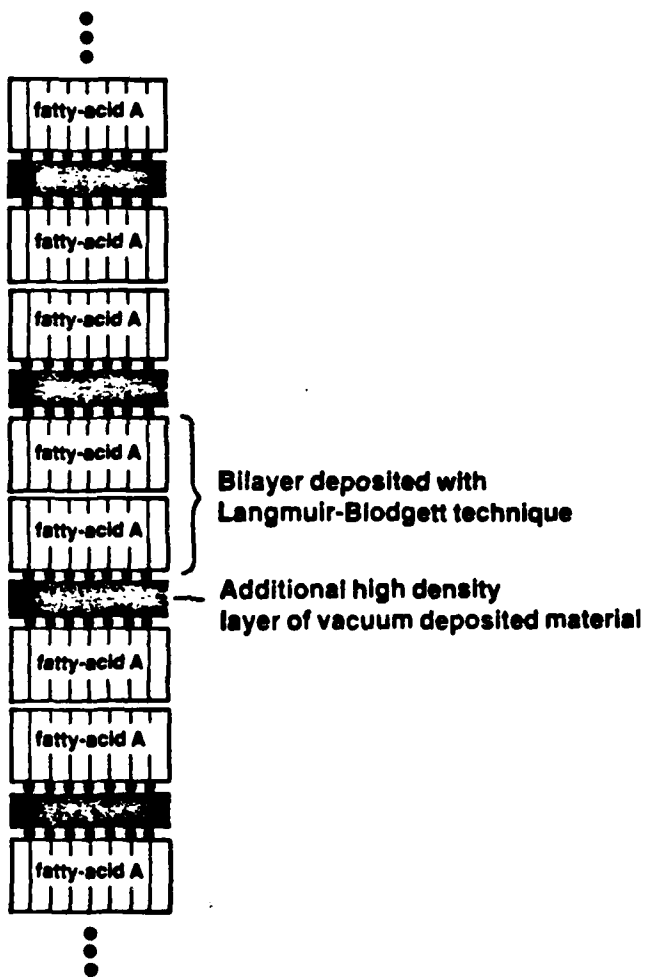


X178

Figure 15

A HYBRID MULTILAYER CONTAINING
LANGMUIR-BLODGETT AND VACUUM DEPOSITED LAYERS

UR
LLE



X179

Figure 16

LANGMUIR TROUGH AND DIPPING APPARATUS

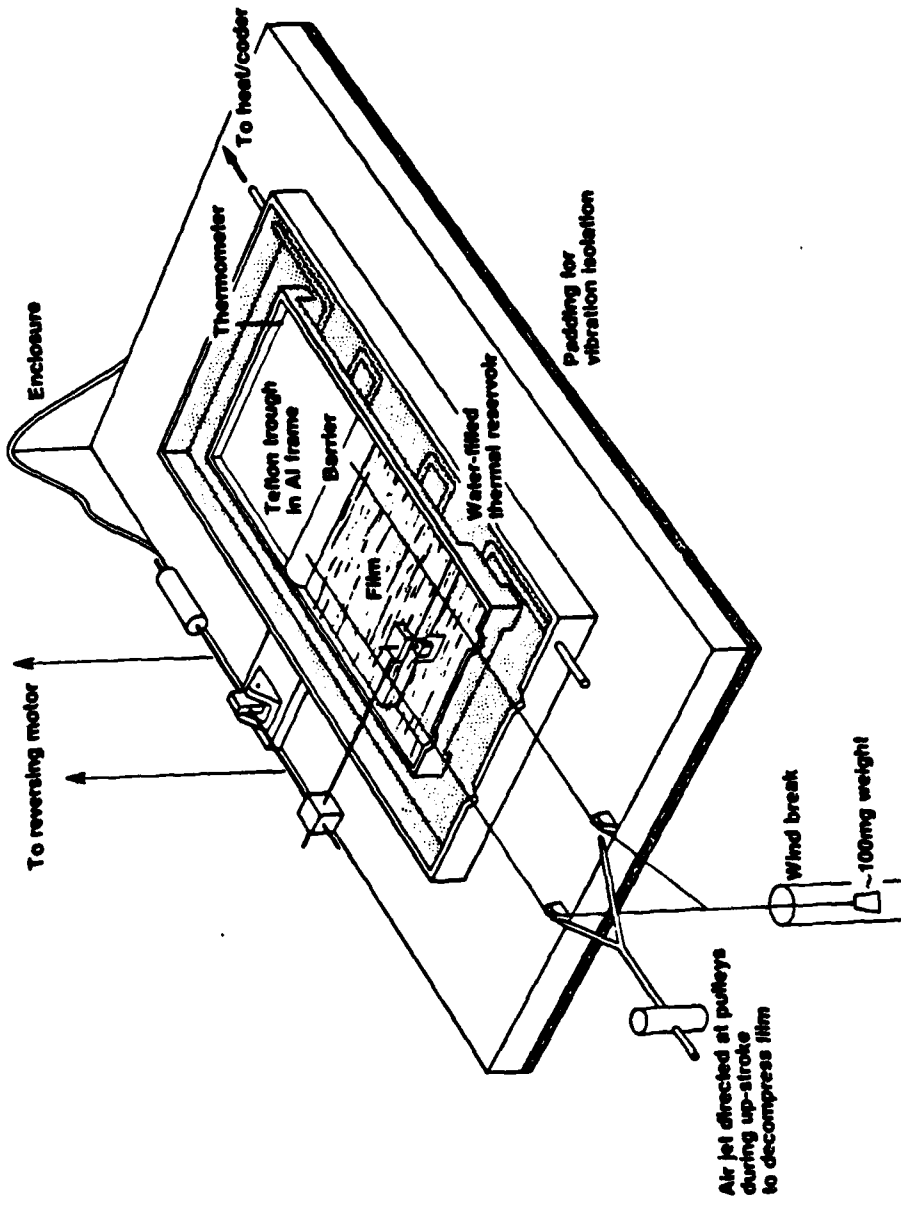


Figure 17

Caption to Figure 17

The pool of water that supports the film is contained in a Teflon-coated Al trough. The water is doubly distilled, and can be cooled or heated relative to the surrounding environment.

The film is compressed by a force supplied to a moveable barrier through weights. The barrier is made of sheet Teflon and "floats" on the water surface. It is slightly wider than the trough but is not in contact with the trough edge; instead it rides on a thin layer of water pinched between the trough edge and itself.

The seesaw-like device that dips the substrate into the film is powered by a reversing motor (not shown; the motor is mounted on a separate table for vibration isolation).

Deposition occurs primarily on the down-strokes, but poor quality up-stroke depositions can take place during the first few cycles. To inhibit these, a jet of air is directed at the pulleys during the up-strokes in order to decompress the film.

The Teflon trough and aluminum supporting frame rest in a water-filled thermal reservoir cooled or heated by a NESLAB RTE-3 circulator.

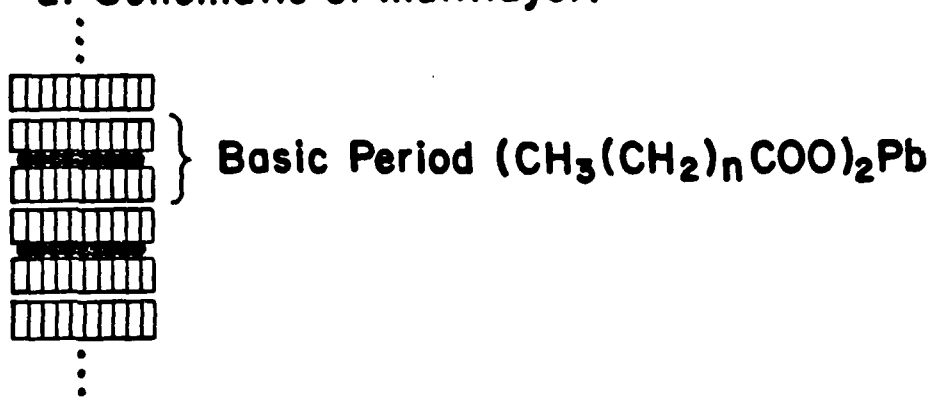
The apparatus is surrounded by a plexiglass enclosure with optional nitrogen-purging, and is mounted on a layer of padding for vibration-isolation. The Teflon parts are cleaned with chromic acid between fabrication sessions.

on each upstroke, and the bilayer molecular alignment shown in Figure 18 is obtained. A multiple bilayer structure is then formed as the dipping of the substrate into the aqueous suspension is repeated.¹⁹ These structures can provide significant normal incidence reflection only at a set of discretely spaced soft x-ray wavelengths corresponding to the discrete set of fatty acid molecular chain lengths. Furthermore, the low concentration of heavy ions in the metallic salts of fatty acids implies that a large number of layers must be used to achieve good reflectivity. This increase in the number of required layers causes an accompanying increase in absorption, reducing the reflectivity finally obtained.

In the structure described in Figure 15, the wavelength of peak reflectivity has been shifted away from any of the discrete values that a mirror made from a single fatty acid molecule would be restricted to; this has been accomplished by periodically inserting into the structure layers formed from a second species of fatty acid. Increased spacings between the metallic layers can be obtained by transferring some of the fatty acid films from an aqueous substrate not containing metallic ions. The effective period thickness of the structure then becomes approximately the arithmetic mean of all spacing distances in the structure's physical repeat period. Since good performance is obtained from such structures over a small but finite range of wavelengths, a limited set of molecular combinations can provide high reflectance over all wavelengths in the 70 \AA - 300 \AA range. (The upper limit simply represents the approximate short wavelength cutoff of conventional reflectors.)

Langmuir-Blodgett Multilayer

a. Schematic of multilayer.



b. Schematic of basic period.

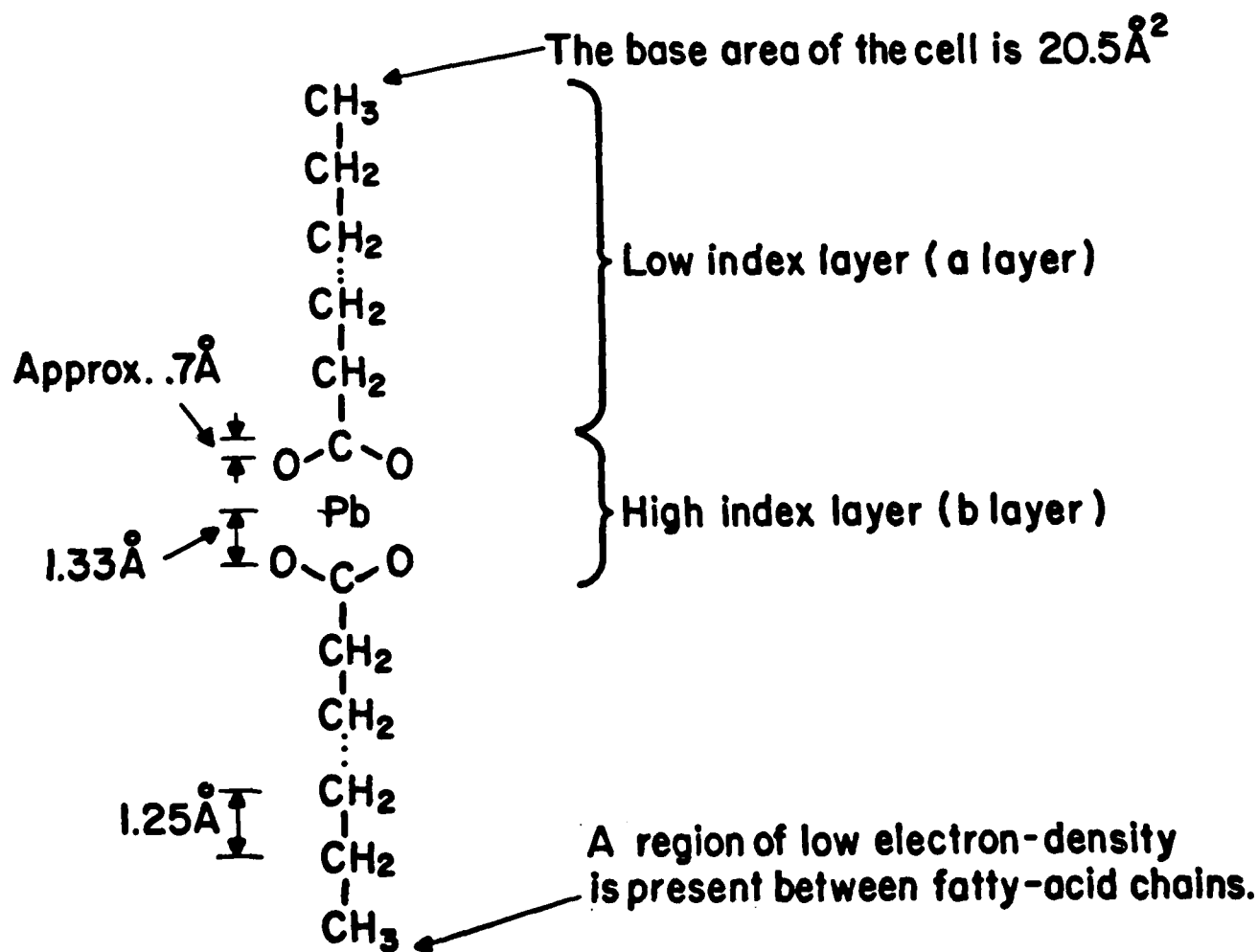


Figure 18

The reflectance of such structures is further enhanced if an additional thin metallic layer is deposited on each monatomic metallic layer that is deposited with the Langmuir-Blodgett technique (Figure 16). This increases the interaction of each individual period with the x-rays, allowing the use of fewer periods in the mirror and consequently the production of mirrors having reduced absorption. If additional metallic layers are used, the resonant wavelength of the mirror can be controlled through variation of the thickness of these layers, rather than through the use of fatty acids having non-uniform molecular lengths.

We have developed an analytic theory of the reflectance of such multilayer structures from which characteristics of the above designs were deduced. For convenience in illustrating the behavior of these structures, we present numerical calculations of the reflectances of typical systems using the MULTFILM III program²⁰. In this program each material layer is assigned a complex index of refraction which is assumed to be constant throughout the layer. Maxwell's equations in such a structure are then solved in a matrix formulation by matching the boundary conditions across the layers.

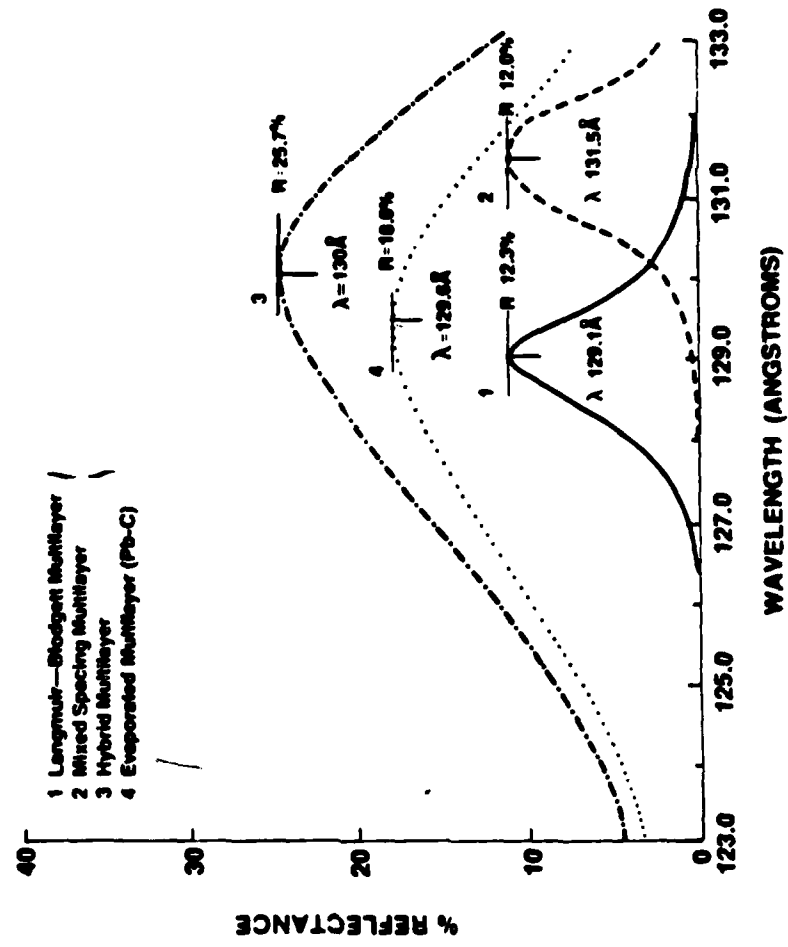
In order to use the program, the material indices of refraction must be determined. The basis for this determination is the atomic model of the fatty acid structures developed by Henke^{21,22}. The complex atomic scattering factors for the atoms are then obtained using various sources. For O and H the imaginary part (f'') is obtained from the Atomic Data Tables²³. The f'' 's for C and Pb change rapidly in the 130 \AA region and values for these were obtained from Tukirskii²⁴ and from DESY²⁵.

The real part (f') for H was calculated assuming free electron scattering. The f' 's for C and O were obtained from DESY data²⁵, the latter values by comparing results for Al and Al_2O_3 . For Pb, f' was obtained from a Kramer's-Kronig calculation by Henke²⁶.

The high index layer is modeled as lying between the terminating carboxyl groups of the fatty acid. The low index layer may be treated as a spatially uniform contribution of CH_2 groups for simplicity; however, a region of low electron density may exist between the facing carbon atoms of the terminal CH_3 groups. Our calculations show that the effect of such a region is to enhance the overall reflectance of the multilayer structure while leaving unchanged the performance trends implied by the use of mixed spacing or hybrid assemblies.

The comparative performance calculated for four types of these multilayer structures is shown in Fig. 19. Curve 1 shows the spectral variation of the normal incidence reflectivity of an ideal (i.e. defect free) multilayer made from lead lignocerate. Included in the calculation was the effect of the postulated low index layer between the fatty acid chains. In curve 2, every fourth molecule in the lignocerate multilayer has been replaced by a molecule of cerotic acid, which has two additional CH_2 groups in the chain. In curve 3, the reflectance of a pure palmitic acid multilayer has been enhanced by deposition of additional metallic lead after each bilayer deposition. The lead density was taken to be half of the bulk metal and to have total thickness of approximately 22 \AA . The attractiveness of the use of hydrocarbons to obtain low index

COMPARISON OF REFLECTIVITIES



X239

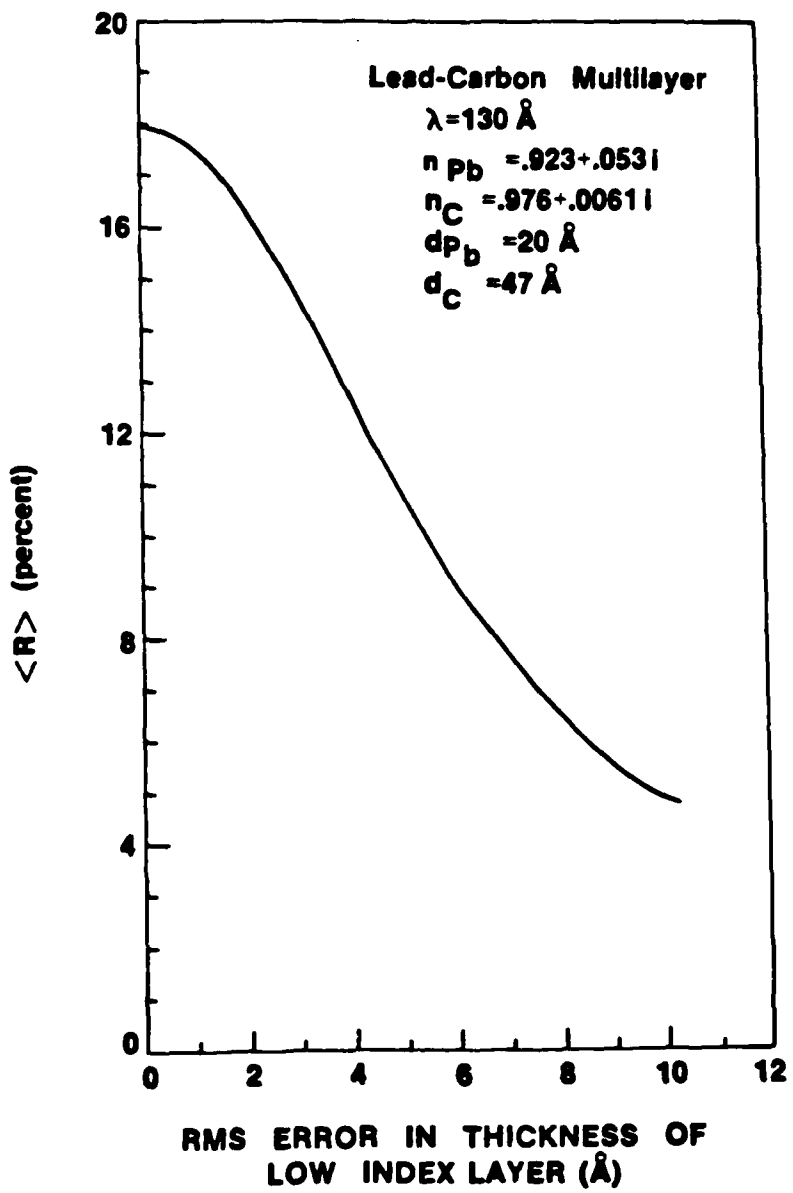
Figure 19

layers is shown in curve 4 where the reflectance of an evaporated structure of alternating pure lead and pure carbon layers of suitably optimized thickness is shown.

A further advantage to the use of the Langmuir-Blodgett fabrication technique is the reproducibility of layer thickness which should be achievable. Although improved methods of controlling the thickness of ultra-thin evaporated layers are being developed, the effect of very small thickness errors can be very serious in reflector performance. The calculated effect on the peak reflectance of randomly distributed thickness errors in the low index layer of the lead-carbon evaporated multilayer shown in Fig. 19, curve 4, is shown in Fig. 20.

THE EFFECT OF DEPOSITION ERROR ON REFLECTIVITY

UNP
L11



X241

Figure 20

VI. REFERENCES

1. L. I. Gudzenko and L. A. Shelepin, *Soviet Physics Doklady* 10, 147 (1965).
2. A review of this work has been given by A. W. Ali and W. W. Jones, *NRL Memorandum Report 3015*, U. S. Naval Research Laboratory, Washington, D. C., 1975.
3. F. E. Irons and N. J. Peacock, *J. Phys.* B7, 1108 (1974); also, R. J. Dewhurst et al., *Phys. Rev. Letters* 37, 1265 (1976).
4. V. A. Bhagavatula and B. Yaakobi, *Opt. Comm.* 24, 331 (1978).
5. R. C. Elton, "Atomic Processes" in *Method of Experimental Physics*, Vol. 9A, edited by H. R. Griem and R. H. Loveberg (Academic Press, New York, 1970) pp. 154-159.
6. E. B. Goldman, *Plasma Physics* 15, 289 (1973).
7. R. W. P. McWhirter, "Spectral Intensities", in *Plasma Diagnostic Techniques*, editors R. H. Huddlestone and S. L. Leonard (Academic Press, New York, 1965) p. 201.
8. H. J. Kunze, A. H. Gabriel and H. R. Griem, *Phys. Fluids* 11, 662 (1968).
9. R. D. Cowan, Los Alamos Scientific Laboratories, private communication.
10. P. A. Slaymaker, "Angular Distribution of Amplified Spontaneous Emission - A Comparison of Theory and Laser-Pumped Dye Amplifier Experiment", Ph.D. thesis, University of Rochester (1978).
11. D. H. Sampson, "Radiative Contributions to Energy and Momentum Transport in a Gas", (Interscience Publishers, New York, 1965).

VI. REFERENCES (continued)

12. E. Spiller, *Appl. Phys. Letters* 20, 365 (1972); also, E. Spiller, *Appl. Optics* 15, 2333 (1976).
13. R. P. Haelbich and C. Kunz, *Opt. Comm.* 17, 287 (1976).
14. A. V. Vinogradov and B. Ya. Zeldovich, *Appl. Optics* 16, 89 (1977).
15. K. B. Blodgett and I. Langmuir, *Phys. Rev.* 51, 964 (1937).
16. B. L. Henke, *private communication*.
17. B. L. Henke and M. A. Tester, "Techniques of Low Energy X-Ray Spectroscopy" in *Advances in X-Ray Analysis*, ed. D. J. Nagel (Plenum, New York, 1975) pp. 76-106.
18. AFOSR Annual Technical Report, Grant 77-3189, Dec. 31, 1978.
19. G. L. Gaines, Jr., Insoluble Monolayers at Liquid-Gas Interfaces, Interscience, 1966.
20. We are grateful to Professor P. W. Baumeister for the use of this program in connection with this research.
21. B. L. Henke et al., *J. Appl. Phys.* 49, 480 (1978).
22. B. L. Henke et al., *Advances in X-ray Analysis* 18, 76 (1974).
23. W. J. Veigle, *Atomic Data* 5, 51 (1973).
24. A. P. Lukirskii et al., *Sov. Phys. Solid State* 8, 1525 (1966).
25. H. J. Hagemann, W. Gudat, C. Kunz, *Internal Report DESY SR-74/7*

VI. REFERENCES (continued)

(1974).

26. B. L. Henke et al., Technical Report, AFOSR 72-2174 (1974).

APPENDIX 1

Volume 24 Number 3

OPTICS COMMUNICATIONS

March 1978

DIRECT OBSERVATION OF POPULATION INVERSION BETWEEN Al^{+11} LEVELS IN A LASER-PRODUCED PLASMA

V.A. BHAGAVATULA and B. YAAKOBI
*Laboratory for Laser Energetics, University of Rochester,
Rochester, New York 14627, USA*

Received 23 December 1977

Measured X-ray intensities of the resonance line series of Al^{+11} in a laser-produced plasma shows population inversion between the $n = 4, 5$ levels and the $n = 3$ level at a plasma density $N_e \sim 10^{20} \text{ cm}^{-3}$. The cooling of the expanding plasma leading to inversion is enhanced by a special target configuration. The gain coefficient in the $4 \rightarrow 3$ transition at 129.7 Å is estimated to be $\sim 10 \text{ cm}^{-1}$, using both measured line intensities and numerical simulation.

Population inversion in an expanding laser-produced plasma has been reported in two previous experiments [1,2]. Here we report on the observation of population inversion of the levels $n = 3$ and 4 (also of $n = 3$ and 5) of Al^{+11} by measuring the X-ray lines from these levels to the ground state. Even though the basic mechanism producing the inversion (i.e., recombination in an expanding plasma) is the same, there are several important differences between this and previous experiments:

(1) Here the observed line ($1s^2 - 1s4p$) starting on the upper level is actually stronger than the line ($1s^2 - 1s3p$) starting on the lower level of the inverted pair, beyond a certain distance from the target. This means that the deduced population inversion is not subject to doubts due to the imprecise knowledge of film calibration. Similar evidence was reported recently by Dixon and Elton [3] in a different inversion scheme: resonant charge exchange.

(2) Our spectra represent a single experiment per exposure.

(3) By employing a laser of power one to two orders of magnitude higher, we were able to achieve inversion in a higher-Z target (Al as compared with C). Consequently, we observe an inversion at a higher density, $N_e \sim 10^{20} \text{ cm}^{-3}$, as compared with $\sim 10^{17} \text{ cm}^{-3}$ in ref. [1] and $\sim 10^{19} \text{ cm}^{-3}$ in ref. [2]. Higher densities lead, of course, to a higher gain.

(4) We employ a full-fledged hydrodynamic numer-

ical code rather than a similarity model as in refs. [2] and [4], and we come to different conclusions: cylindrical expansion is not really advantageous over planar expansion. The expanding plasma in both cases goes through a similar succession of parameter values (temperature, density, population), only in plane expansion this is extended over longer time and distance spans.

(5) The most important feature of the present experiment is the employment of a stepped target designed to cool the plasma at a certain distance from the initial surface. The idea here is that unlike expansion, cooling due to an additional plate is not accompanied by a drop in density and with it in gain.

Fig. 1 shows the experimental configuration: a glass:Nd laser of energy typically 10 J in 200 ps is

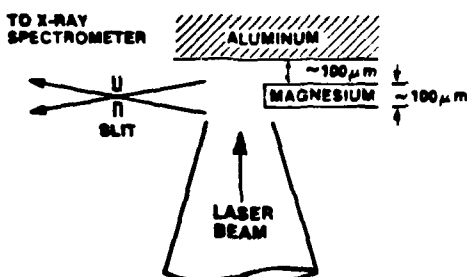


Fig. 1. The experimental configuration.

focused onto a stepped target: an aluminum slab and a magnesium plate in front of it for cooling the expanding Al plasma. Magnesium was chosen because Al and Mg lines can be registered on the same film. A small portion of the laser beam hits the magnesium plate giving rise to weak emission of the two resonance lines of Mg^{+10} and Mg^{+11} ions. The high density Mg plasma close to the Mg plate surface where the temperature drops to the metal bulk temperature is a heat sink, drawing heat from the low density high temperature Al expanding plasma. An X-ray crystal spectrograph equipped with a slit measured Al and Mg lines as a function of the distance perpendicular to the target. Spectra registered on Kodak No-Screen and Kodak RAR2490 films gave very similar results except that the latter film has a better signal to background ratio. Elaborate calibration of No-Screen film has been carried out in our laboratory [5] whereas for RAR2490 film we relied on the curves given by

Benjamin et al. [6]. The reflectivity of the analyzing crystal (Ti.A.P.) was measured by Henke and Tester [7].

Fig. 2 shows the aluminum spectra before calibration at two distances from the aluminum surface. The line $1s^2 - 1s4p$ was found to be consistently stronger than the $1s^2 - 1s3p$ line for all distances $\geq 300 \mu\text{m}$, showing unequivocally an inversion between the $n = 4$ and 3 levels. For larger distances ($\geq 500 \mu\text{m}$) even the line $1s^2 - 1s5p$ becomes more intense than the two preceding ones. For smaller distances but larger than $150 \mu\text{m}$ we derive population inversion of the $n = 3, 4$ levels even though the line intensities themselves decrease along the series. Flat (non-stepped) targets of Al or Mg do not show such intensity inversion (even though some population inversion was deduced). This behavior is consistent with recombination in a cooling plasma which will show population inversion if $N_e \leq 10^{14} Z^7$ (so that excitation colli-

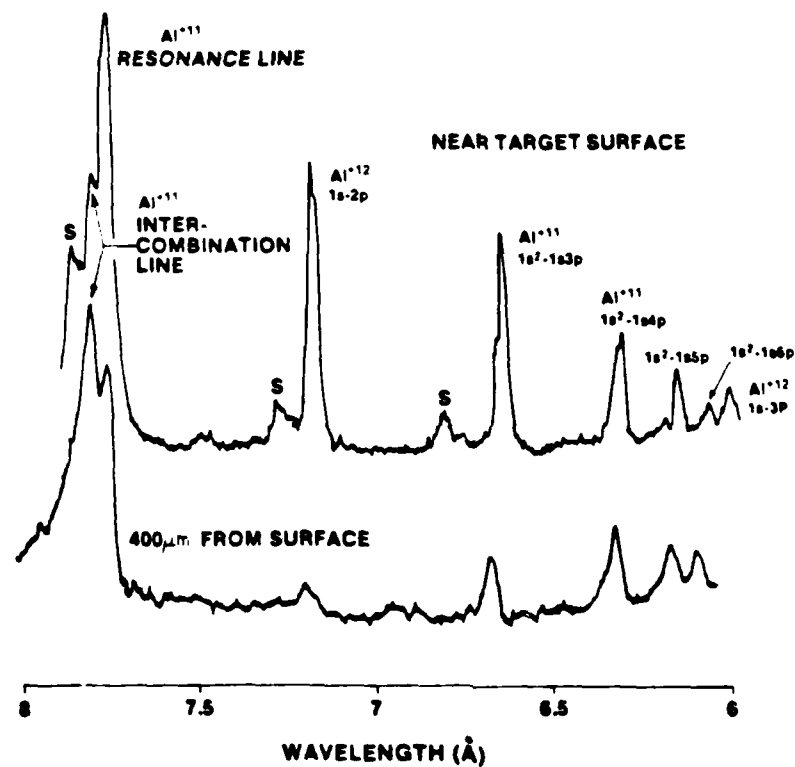


Fig. 2 Single-shot aluminum spectra from a stepped target (spatial resolution $50 \mu\text{m}$). The lower spectrum shows inversion of the $(1s3p, 1s4p)$ pair. S denotes dielectronic satellites. These are plots of film density with different scales (see also fig. 3).

sions are unimportant [8]), the temperature is sufficiently low and the density ratio $Q = n(\text{Al}^{+12})/n(\text{Al}^{+11})$ is sufficiently high. This implies the relative "freezing" of the Al^{+12} ion density which provides the pumping source for the inversion.

We compare the experimental results with the one-dimensional two-temperature hydrodynamic code SUPER [9] which includes an atomic physics group of subroutines similar to what is described in ref. [4]: rate equations for the evolution of Al ions charge states and excited level populations, and the escape factor approximation for line radiation transport. Using code calculations (and the experimental results), the opacity of the $1s^2-1s3p$ and $1s^2-1s4p$ lines can be estimated and it turns out to be much smaller than 1 at the large distances where inversion is observed (along the narrow dimension of the plasma). Opacity effects can then by no means account for the observed intensity inversion.

Fig. 3 shows that the plasma expands in a narrow axial channel (this was also found by Feldman et al. [10]): line widths obtained by the non-focusing spectrograph are determined by the source width. Fig. 3 indicates a plasma width $\lesssim 200 \mu\text{m}$ over a large distance ($> 500 \mu\text{m}$) from the target. A numerical simulation assuming a planar expansion is therefore justified. Also, the lines intensity decay with distance is

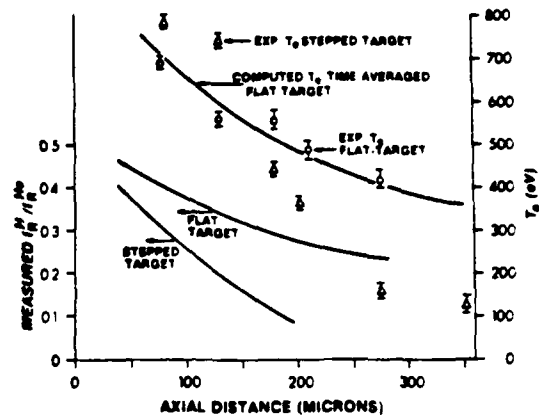


Fig. 4. Computed and measured electron temperature as a function of distance from the aluminum surface. Triangles denote experimentally determined temperature values for the stepped target of fig. 1, circles for a flat aluminum target. Lower curves: measured intensity ratios of the resonance lines of hydrogen-like to helium-like aluminum ions.

found to be consistent with planar, but not hemispherical expansion.

Fig. 4 compares measured and computed profiles of T_e . The measured intensity ratio of the Al^{+12} to Al^{+11} resonance lines drops faster with distance when the Mg plate is added. This is evidence of addi-

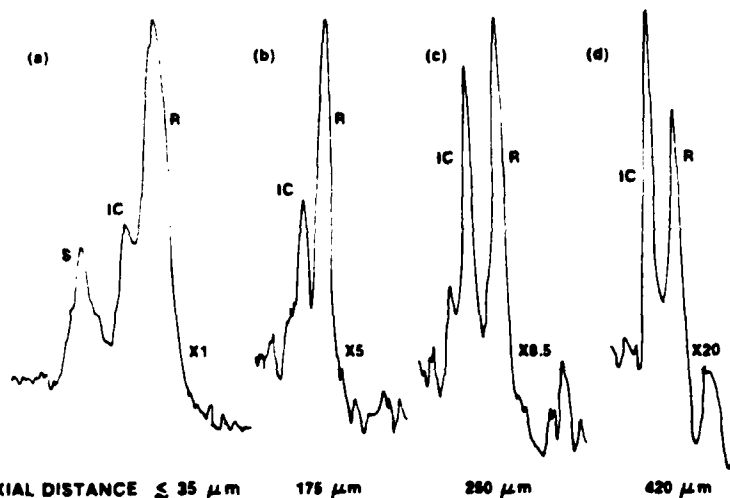


Fig. 3. Film density traces of Al^{+11} lines used to determine the plasma density profile. R: $1s^2-1s^2p^1P$, IC: $1s^2-1s2p^3P$. S denotes dielectronic satellites. Note that the curves have slightly different horizontal scales and different height scale factors. Spatial resolution was $38 \mu\text{m}$.

tional cooling due to the plate. For the recombination regime pertinent to our case simple coronal or LTE models are not relevant in determining the electron temperatures. The experimental electron temperatures are derived using the more appropriate steady state excited level model of ref. [8] by comparing the observed intensity ratio of the inverted lines to the tabulated values. As fig. 4 shows, the values thus derived are consistent with the code predictions. The intensity of each resonance line is affected by opacity but the ratio is relatively independent of absorption. However, the addition of the Mg plate causes T_e to fall faster with distance. To model this cooling in the code we assumed a lateral temperature gradient scale of 200μ conducting heat into a sink of $N_c = 10^{21} \text{ cm}^{-3}$ at a location corresponding to the Mg plate. This is an approximate model designed only to show qualitatively the effect of additional cooling.

Fig. 5 shows the ratio of reduced populations (i.e., after division by the statistical weights) for the $n = 3, 4$ shells derived from the measured intensities of the lines $1s^2 - 1s3p$ and $1s^2 - 1s4p$. The electron density is derived from the intensity ratio of the resonance line and the intercombination line (R and IC in fig. 3), using cross-sections given by Vinogradov et al. [11]. We see that inversion exists in a region where N_e is of order 10^{20} cm^{-3} . Neglecting opacity of the resonance line yields a conservative estimate of N_e (and the gain) and is probably responsible in part for the

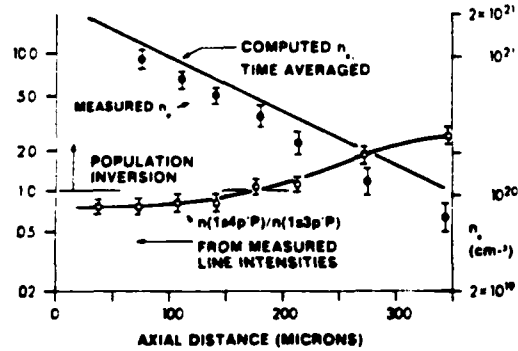


Fig. 5. Upper curve: comparison between computed and measured electron density profile. Measured values (full circles) are derived from I_R/I_{IC} values (fig. 3). Lower curve: the line through the open circles denotes reduced population ratio of the inverted level pair as deduced from the measured line intensities.

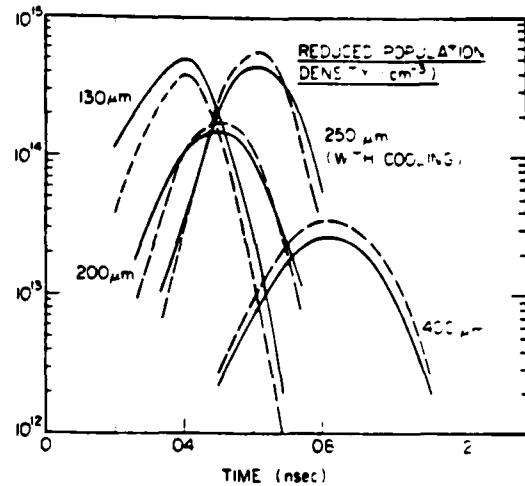


Fig. 6. Numerical code calculation of reduced population densities. Distances are from initial aluminum surface. The pair of curves at $250 \mu\text{m}$ corresponds to a calculation with provision to simulate the cooling effect of the magnesium plate. The other three pairs correspond to a simple flat aluminum target.

experimental N_e points being lower than the calculated curve.

Finally, we show in fig. 6 a sample calculation of population density evolution, with and without additional cooling. There is no inversion at $130 \mu\text{m}$ because the streaming plasma arrives there, first, with too high a temperature, then with too low a Q . On the other hand, plasma conditions are right to obtain small inversion at $200 \mu\text{m}$ and $400 \mu\text{m}$. Notice that enhanced cooling (the curves at $250 \mu\text{m}$) increases the peak reduced inversion density by a factor of 4 to 5 (compare with curves at $200 \mu\text{m}$) and also increases the population ratio of the inverted level pairs. This agrees with the fact that with a stepped target large population ratios and even intensity inversions of the inverted level pair are observed. Fig. 6 also shows that spatial resolution at these distances is partially equivalent to temporal resolution. Using either the calibrated line intensities or the curves "with cooling" in fig. 6, we estimate the gain coefficient for the $4^3F - 3^3D$ manifold [12] at 129.7 \AA to be $\sim 10 \text{ cm}^{-1}$ which for the measured plasma width $\sim 200 \mu\text{m}$ yields a gain of $\exp(0.2)$.

In conclusion, we find that plasma expansion far from a flat target is one-dimensional and shows popu-

lation inversion via recombination. The addition of a plate in front of the target is found both to cool the plasma and to increase the inversion to give an average gain coefficient of $\sim 10 \text{ cm}^{-1}$. A one-dimensional simulation code was able to reproduce quite well the experimental results (figs. 4 and 5). The present experimental arrangement brings us much closer to being able to observe gain in soft X-ray transitions.

The authors gratefully acknowledge the continuous guidance and intensive discussions with Professors J. Forsyth and M.L. Lubin. Portions of this work were supported by the Air Force Office of Scientific Research under grant (AFOSR-77-3) 189.

References

[1] F.E. Irons and N.J. Peacock, *J. Phys. B* 7 (1974) 1109.

- [2] R.J. Dewhurst et al., *Phys. Rev. Letters* 37 (1976) 1265.
- [3] R.H. Dixon and R.C. Elton, *Phys. Rev. Letters* 38 (1977) 1072.
- [4] G.J. Pert, *J. Phys. B* 9 (1976) 3301.
- [5] A. Hauer and G. Harvey, *Soft X-ray calibration of no-screen film*, Tech. Note No. 2, X-Ray Group, LLE, University of Rochester (1975).
- [6] R.F. Benjamin et al., *Appl. Optics* 16 (1977) 393.
- [7] B.L. Henke and M.A. Tester, *Adv. in X-Ray Analysis* 18 (1975).
- [8] R.P. McWhirter and A.G. Heran, *Proc. Phys. Soc. London* B82 (1963) 641.
- [9] E.G. Goldman, *Plasma Physics* 15 (1973) 289, and University of Rochester, LLE Report #16 (1974) (unpublished).
- [10] U. Feldman et al., *J. Appl. Phys.* 47 (1976) 1341.
- [11] A.V. Vinogradov et al., *Sov. J. Quantum Electron.* 5 (1975) 630; a revised version in *Preprint* 121, Lebedev Institute (1977).
- [12] R.D. Cowan, Los Alamos Scientific Lab., private communication.

APPENDIX 2

ABSTRACT FROM:

Angular Distribution of Amplified Spontaneous Emission -
A Comparison of Theory and Laser-Pumped Dye Amplifier Experiment

by

Philip Arthur Slaymaker

Submitted in Partial Fulfillment

of the

Requirements for the Degree

Doctor of Philosophy

Supervised by Dr. James Forsyth

Institute of Optics

The University of Rochester

Rochester, New York

1978

NOTE: Full text of this thesis contained in the Annual Technical Report for AFOSR Grant 77-3189, 1 November 1977 - 31 October 1978.

Abstract

Amplified spontaneous emission (ASE) is stimulated emission initiated by the fluorescence in a laser amplifier in the absence of optical feedback. A measurement of the angular distribution of ASE is shown to be a practical, sensitive, and unambiguous single-shot diagnostic of gain in laser amplifier experiments. The technique is more sensitive than spectral line narrowing observations in situations in which the measurements are spatially integrated. ~~Other direct measurement techniques, such as pulse injection or gain-length variation, are often impractical because of the lack of reproducibility of the (pulsed) experimental conditions.~~

A two-dimensional geometric model is presented that predicts the angular distribution of ASE from a rectangular amplifier with uniform fluorescence and gain. The radiation transport equation including gain is integrated over the amplifier to determine the total radiant intensity emitted into a given direction. Angular distribution curves are presented in terms of the amplifier length to width ratio and the gain-length product. The FWHM beam divergence is shown to be inversely proportional to the amplifier aspect ratio and to increase with decreasing gain-length product. Near threshold the beam divergence is several times larger than the inverse aspect ratio. Calculations for integrated measurements in which the gain coefficient and fluorescence rate are linear functions of a parameter (time, wavelength, space) show that an average gain coefficient may be used in the uniform gain model to good approximation at small

gain-length products. A reasonable threshold for the determination of gain from directional ASE measurements is found to occur for an average gain-length product of unity.

A transverse laser-pumped dye amplifier experiment is described which was designed to measure the ASE angular distribution from an optically freestanding amplifier with a non-uniform transverse gain profile. Measurements of the distribution are presented, and the observed dependence on the gain coefficient and the amplifier geometry compared to that predicted by the ASE theory. To simulate an optically freestanding amplifier, R6G dye was index matched to its cell, thus suppressing reflections and parasitic oscillations. The dye concentration determined the transverse gain profile. Pumping was provided by a frequency-doubled 15nsec. pulse from a Q-switched $^{+3}\text{Nd}:\text{Yag}$ oscillator and $^{+3}\text{Nd}:\text{glass}$ amplifier chain.

In order to simulate an inhomogeneous laser-produced plasma x-ray amplification experiment, the model is extended to the case where only a portion of the emitting region exhibits gain. The result is that the direction of greatest intensity shifts off of the amplifier axis, and the overall directionality is reduced at a given gain-length product. The directionality of ASE is shown to still provide a useful diagnostic of gain under such conditions.

APPENDIX 3

Summaries of papers presented at the Annual Meeting of the Optical Society of America, October 8-12, 1979, Rochester, New York.

EUV AND X-RAY SPECTROSCOPY OF AN INVERTED LASER-PRODUCED ALUMINUM PLASMA*

Yves Conturie and J. M. Forsyth

An aluminum plasma produced by a point-focus Nd^{3+} -Glass laser (500 psec, up to 100 J) is cooled at an early stage of its expansion by a "heat sink," a metallic foil placed near the surface of the Al target.¹ High electron density and low temperature increase the probability of recombination through three-body rather than radiative processes, favoring the population of high-lying quantum states.² Two spatially resolving crystal-spectrographs at perpendicular directions provide three-dimensional information on the transitions to the ground-state in the H-like and He-like stages of the plasma. Two target geometries show evidence of population inversion between several Al⁺¹¹ levels and possibly between the n=4 and 3 Al⁺¹² levels: (i) a magnesium slit in front of an aluminum slab at normal incidence, (ii) a magnesium sheet on the side of a tilted aluminum slab. A grazing-incidence grating spectrograph is used for direct observation of the inverted transitions. Single-shot Al spectra in the range 50 Å - 500 Å are presented. Single-shot Fe spectra recorded under the same conditions provide a reference for the line identification. Preliminary results on line-focus experiments (using a cylindrical lens) are also presented.

*Research Supported, in part, by AFOSR Grant 77-3189.

¹Bhagavatula and Yaakobi, Opt. Comm. 24, 331 (1978).

²McWhirter and Hearm, Proc. Phys. Soc. 82, 641 (1963).

NORMAL INCIDENCE SOFT X-RAY REFLECTORS FOR
ARBITRARY WAVELENGTHS USING A MODIFIED LANGMUIR BLODGETT METHOD*

Alan E. Rosenbluth and J. M. Forsyth

X-ray reflectors operating near normal incidence must contain a large number of (near) quarter-wave periods due to the weak interaction of x-rays with matter. As a result, the production of such reflectors using conventional layer deposition techniques presents a challenging problem.¹

For wavelengths in the 100 Å regime, the stringent tolerances involved can be met using the Langmuir-Blodgett technique, in which successive portions of a monomolecular fatty-acid film are transferred from an aqueous to a solid substrate.²

The technique may be modified in an effort to produce mirrors tuned to reflect arbitrary source wavelengths. One such modification makes use of mirrors in which different layers are formed from different molecules; another uses mirrors in which the high-index layers formed by the head-groups of the molecules are augmented.

An equivalent-index analysis of such structures indicates that reflectors of the first type have an absorption-limited performance of about 10%; reflectivities of roughly 50% appear to be possible in principle from reflectors of the second type.

Such reflectors might serve as cavity mirrors in an x-ray laser. The technology involved may also be useful in surface-smoothing, and in x-ray astronomy, microscopy, and lithography.

*Research Supported, in part, by AFOSR Grant 77-3189.

¹R.P. Haelbich, A. Segmüller, and E. Spiller, *Appl. Phys. Lett.*, 34 (3), 1979, p. 184.

²G.L. Gaines, Jr., Insoluble Monolayers at Liquid-Gas Interfaces, Interscience, 1966.



**ABSTRACT OF
NEW
TECHNOLOGY
FROM THE AIR FORCE SYSTEMS COMMAND**

APPENDIX 4
PROVIDES INFORMATION ON
THE PRODUCTS OF AFSC
RESEARCH, DEVELOPMENT,
AND TESTING PROGRAMS.



High Reflectance Normal Incidence Mirrors for Arbitrary Soft X-Ray Wavelengths between 70-300Å

Illustrations: Figures 1, 2, and 3 are attached.

Description

We describe a mirror structure that can provide a high normal incidence reflectivity at any chosen soft x-ray wavelength in the range 70Å-300Å, where conventional metallic reflectors cannot function. The new reflector is a modified multiple bilayer structure consisting of a periodic array of fatty acid films separated by thin metallic layers.

Source

Alan Rosenbluth
James M. Forsyth
Laboratory for Laser Energetics
University of Rochester
250 East River Road
Rochester NY 14623

Publications

Alan E. Rosenbluth, "Normal Incidence Reflectors for Soft X-Rays," Institute of Optics, Spring, 1979, Industrial Associates Meeting, Rochester NY, April 25, 1979.

Alan E. Rosenbluth, J. M. Forsyth, "Normal Incidence Soft X-Ray Reflectors for Arbitrary Wavelengths Using a Modified Langmuir-Blodgett Method," Optical Society of America, 1979 Annual Meeting, Rochester NY, Oct. 10, 1979.

A well-known class of periodic structures that satisfy resonant reflectance conditions at certain wavelengths in the range 70 \AA -160 \AA are the Langmuir-Blodgett multilayers. Such a structure is formed by floating a monomolecular fatty acid film on a heavy metal ion solution and then attaching the monolayer to a mirror substrate by dipping the substrate into the solution. A layer is deposited on each downstroke and sometimes on each upstroke, and the bilayer molecular alignment shown in Figure 2 is obtained. A multiple bilayer structure is then formed as the dipping of the substrate into the aqueous suspension is repeated.¹ These structures can provide significant normal incidence reflection only at a set of discretely spaced soft x-ray wavelengths corresponding to the discrete set of fatty acid molecular chain lengths. Furthermore, the low concentration of heavy ions in the metallic salts of fatty acids implies that a large number of layers must be used to achieve good reflectivity. This increase in the number of required layers causes an accompanying increase in absorption, reducing the reflectivity finally obtained.

In the structure described in Figure 1, the wavelength of peak reflectivity has been shifted away from any of the discrete values that a mirror made from a single fatty acid molecule would be restricted to; this has been accomplished by periodically inserting into the structure layers formed from a second species of fatty acid. Increased spacings between the metallic layers can be obtained by transferring some of the fatty acid films from an aqueous substrate not containing metallic ions. The effective period thickness of the structure then becomes approximately the arithmetic mean of all spacing distances in the structure's physical repeat period. Since good performance is obtained from such structures over a small but finite range of wavelengths, a limited set of molecular combinations can provide high reflectance over all wavelengths in the 70 \AA -300 \AA range. (The upper limit simply represents the approximate short wavelength cutoff of conventional reflectors.)

The reflectance of such structures is further enhanced if an additional thin metallic layer is deposited on each monatomic metallic layer that is deposited with the Langmuir-Blodgett technique. This increases the interaction of each individual period with the x-rays, allowing the use of fewer periods in the mirror and consequently the production of mirrors having reduced absorption. If additional metallic layers are used, the resonant wavelength of the mirror can be controlled through variation of the thickness of these layers, rather than through the use of fatty acids having non-uniform molecular lengths.

Present x-ray technology can provide significant reflection of x-rays only at grazing angles of incidence. Recent experimental investigation into the production of x-ray amplifying media suggests that successful fabrication of normal incidence mirrors of moderate reflectivity might make possible the development of x-ray lasers (Figure 3).²

The development of normal incidence x-ray reflecting optics would also be of importance in x-ray microscopy and astronomy, in that it would allow better flux collection, larger fields of view, smaller aberrations and finer diffraction limits than grazing optics. There is some indication that a single Langmuir-Blodgett monolayer is capable of bridging small gaps in an underlying substrate, and a cumulative smoothing may be present when multiple layers are deposited. The control over surface roughness that such a smoothing effect might provide would help increase the resolution of x-ray optical systems and would be of interest in other applications.

The development of normal incidence x-ray reflecting optics would also be of benefit in the study of surfaces and in x-ray lithography.

1. G. L. Gaines, Jr., Insoluble Monolayers at Liquid-Gas Interfaces, Interscience, 1966.
2. V. A. Bhagavatula, B. Yaakobi, Opt. Comm., 24, 3, March 1978, p. 331.

Physical Repeat Period of New Type of X-Ray Mirror

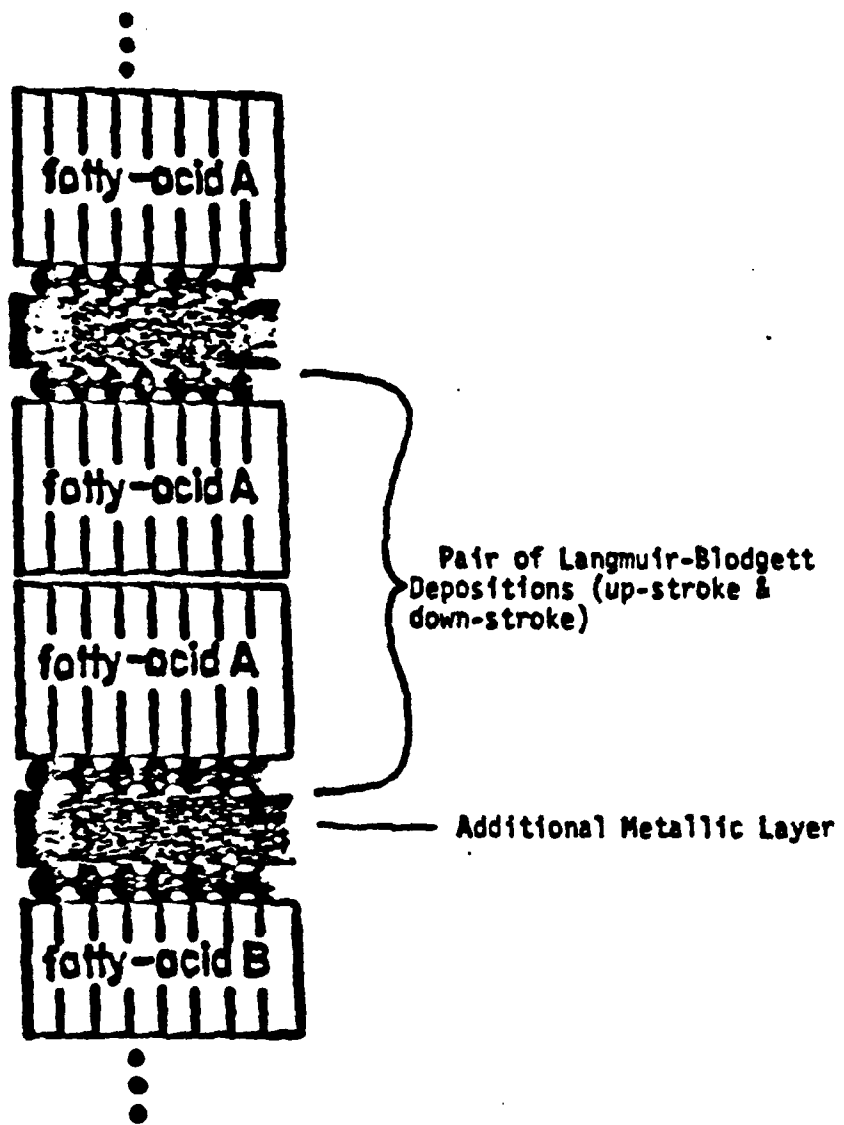
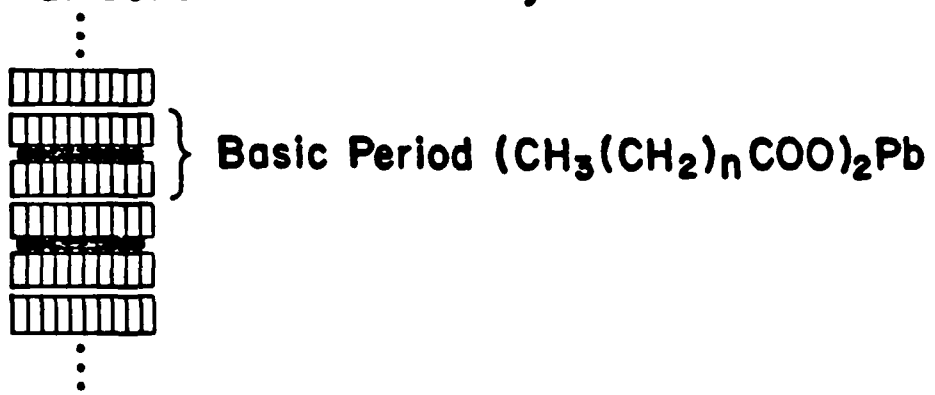


Figure 1

Langmuir-Blodgett Multilayer

a. Schematic of multilayer.



b. Schematic of basic period.

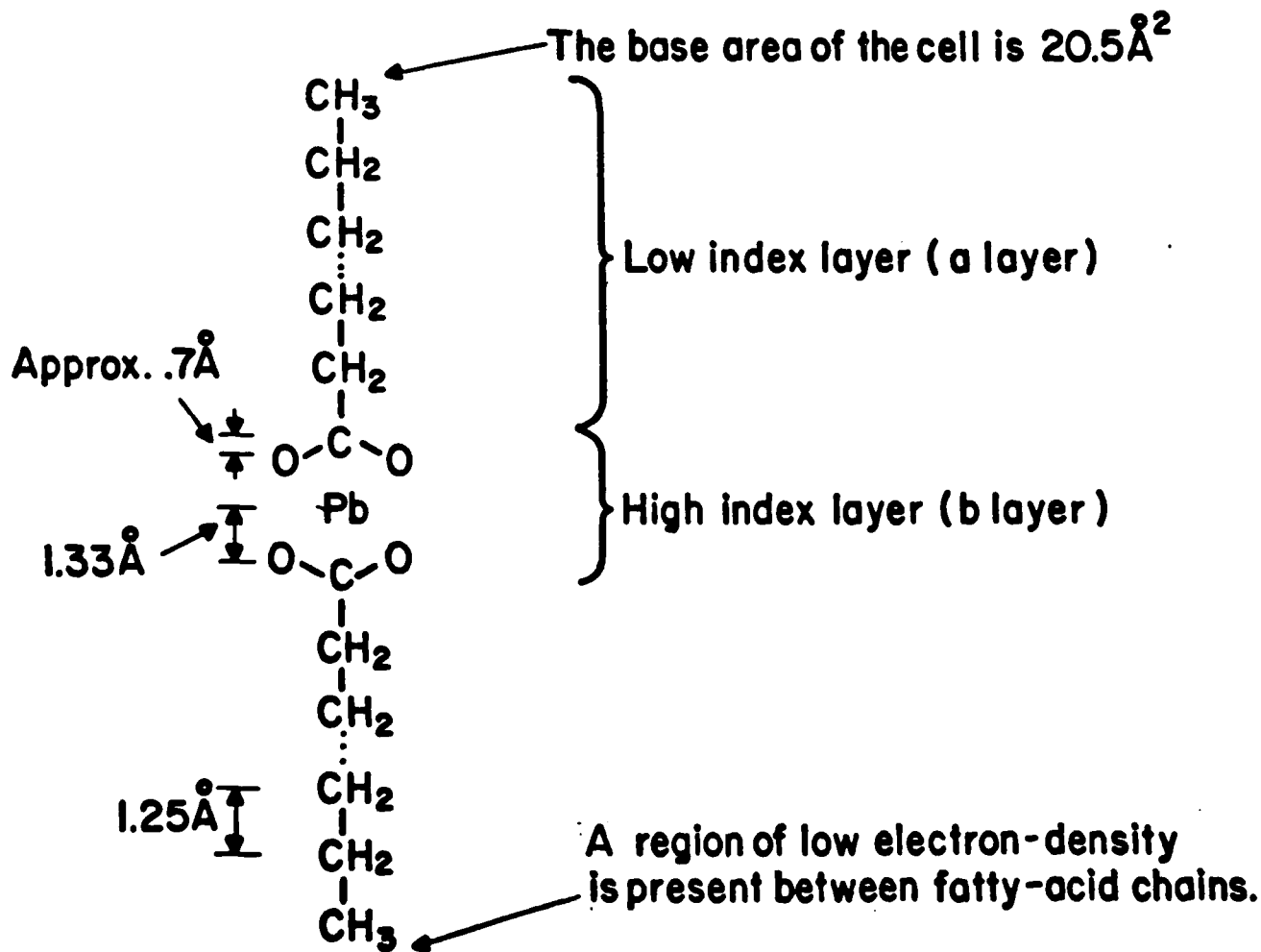


Figure 2

Schematic of Possible X-Ray Laser System

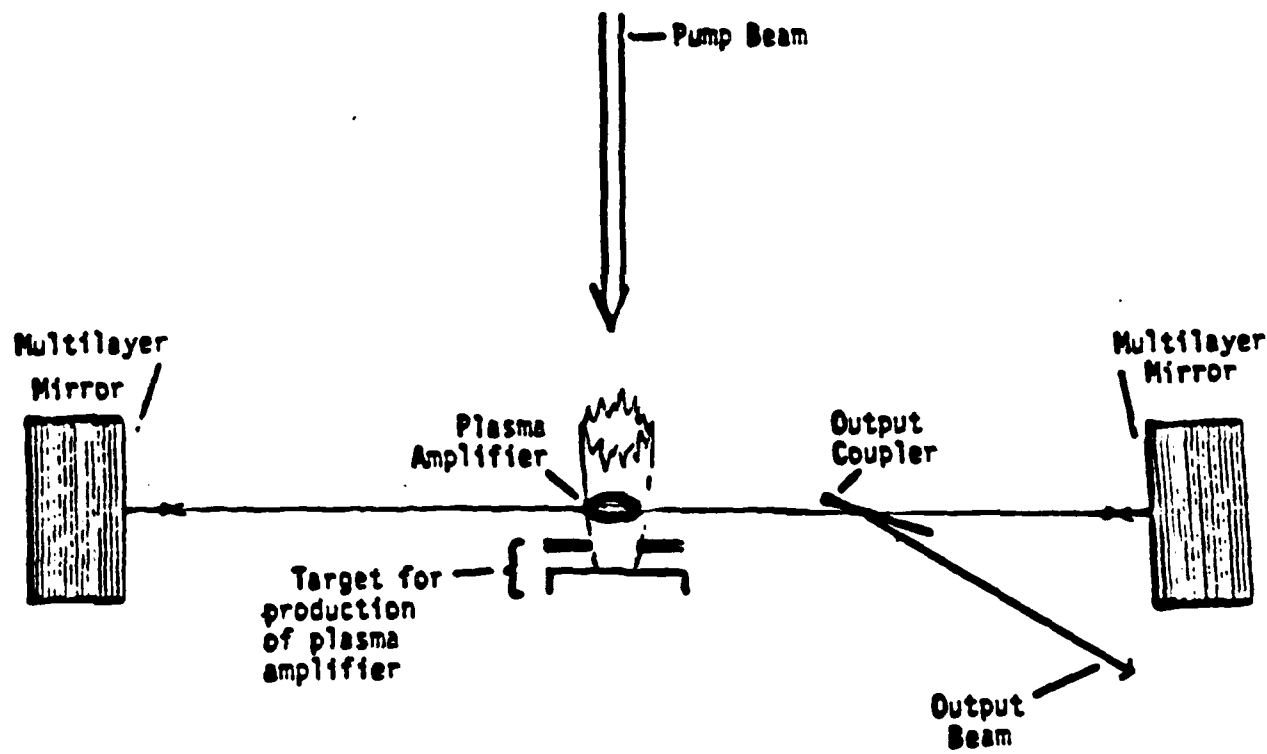


Figure 3

APPENDIX 5

ABSTRACT FOR U. S. PATENT APPLICATION, SERIAL NUMBER 88,699 -
FILED OCTOBER 26, 1979.

Mirror structures are described which provide high normal incidence reflectivities at x-ray wavelengths (such as soft x-ray wavelengths in the range 70 Å to 300 Å) where conventional metallic reflectors can not function. The mirror is made up of an array of repeated periods each consisting of monoatomic metallic layers and Langmuir-Blodgett hydrocarbon molecular layers. The mirror may also include additional Langmuir-Blodgett bilayers serving as spacer layers and/or additional reflection-enhancing metal films. The various layers are systematically deposited in such a way that, first, the mirror structures are periodic, and second, that the average separation between metallic layers maximizes the reflectance at the design wavelength. Such mirror structures can be configured to define a resonant cavity to support x-ray laser action.

ACKNOWLEDGEMENT

In addition to support from AFOSR Grant 77-3189, this work was partially supported by the following sponsors: Exxon Research and Engineering Company, General Electric Company, Northeast Utilities, New York State Energy Research and Development Authority, The Standard Oil Company (Ohio), The University of Rochester, and Empire State Electric Energy Research Corporation. Such support does not imply endorsement of the content by any of the above parties.

END
DATE
FILMED

8-81

DTIC